Myogenin controls via AKAP6 non-centrosomal microtubule organizing center formation at the nuclear envelope

Robert Becker[1], Silvia Vergarajauregui[1], Florian Billing[1], Maria Sharkova[1], Eleonora Lippolis[2], Kamel Mamchaoui[3], Fulvia Ferrazzi[2,4,5,6], Felix B. Engel[1,6,*]

[1]Experimental Renal and Cardiovascular Research, Department of Nephropathology, Institute of Pathology, Friedrich-Alexander-Universität Erlangen-Nürnberg (FAU), 91054 Erlangen, Germany

[2]Institute of Human Genetics, Friedrich-Alexander-Universität Erlangen-Nürnberg, 91054 Erlangen, Germany

[3]Sorbonne Universités UPMC Université Paris 06, INSERM U974, CNRS FRE3617, Center for Research in Myology, GH Pitié Salpêtrière, 47 Boulevard de l'Hôpital, 75013 Paris, France

[4]Department of Nephropathology, Institute of Pathology, Friedrich-Alexander-Universität Erlangen-Nürnberg (FAU), 91054 Erlangen, Germany

[5]Institute of Pathology, Friedrich-Alexander-Universität Erlangen-Nürnberg (FAU), 91054 Erlangen, Germany

[6]Muscle Research Center Erlangen (MURCE), 91054 Erlangen, Germany

Short title: Myogenin controls ncMTOC formation

***Corresponding author:**

Felix B. Engel, Universitätsklinikum Erlangen, Schwabachanlage 12 (TRC), 91054 Erlangen, Germany, felix.engel@uk-erlangen.de

Abstract

Non-centrosomal microtubule organizing centers (MTOC) are pivotal for the function of multiple cell types, but the processes initiating their formation are unknown. Here, we find that the transcription factor myogenin is required in myoblasts for the localization of MTOC proteins to the nuclear envelope. Moreover, myogenin is sufficient in fibroblasts for nuclear envelope MTOC (NE-MTOC) formation and centrosome attenuation. Bioinformatics combined with loss- and gain-of-function experiments identified induction of AKAP6 expression as one central mechanism for myogenin-mediated NE-MTOC formation. Promoter studies indicate that myogenin preferentially induces the transcription of muscle- and NE-MTOC-specific isoforms of *Akap6* and *Syne1*, which encodes nesprin-1α, the NE-MTOC anchor protein in muscle cells. Overexpression of AKAP6β and nesprin-1α was sufficient to recruit endogenous MTOC proteins to the nuclear envelope of myoblasts in the absence of myogenin. Taken together, our results illuminate how mammals transcriptionally control the switch from a centrosomal MTOC to an NE-MTOC and identify AKAP6 as a novel NE-MTOC component in muscle cells.

Keywords: myogenin; muscle differentiation; MTOC; non-centrosomal MTOC; AKAP6; centrosome; microtubules; terminal differentiation; nuclear envelope; transcription

Introduction

Correct organization of the microtubule cytoskeleton is essential for many cellular processes such as the establishment of cell shape, organelle positioning or intracellular transport (Akhmanova & Steinmetz, 2015; Conduit, Wainman, & Raff, 2015). In proliferating vertebrate cells, proteins that control microtubule nucleation and anchoring accumulate as pericentriolar material (PCM) at the centrosome, which in turn functions as the dominant microtubule-organizing center (MTOC) (Prosser & Pelletier, 2015). The centrosomal MTOC is pivotal for cell cycle progression and correct chromosome segregation during mitosis (Hinchcliffe, Miller, Cham, Khodjakov, & Sluder, 2001; Khodjakov & Rieder, 2001; Sir et al., 2013). In contrast, MTOC function is assigned to non-centrosomal sites (ncMTOCs) during differentiation of various cell types (Sanchez & Feldman, 2017). In epithelial cells, apically localized ncMTOCs participate in organelle positioning and help to establish apical-basal cell polarity (Brodu, Baffet, Le Droguen, Casanova, & Guichet, 2010; C. Lee, Scherr, & Wallingford, 2007; Meads & Schroer, 1995; Toya et al., 2016). In neurons, dendritic branch points, Golgi outposts, and pre-existing microtubules have been suggested to act as ncMTOC sites and precise control of microtubule array polarity helps to define the axonal and dendritic compartments (Luders, 2020; Nguyen et al., 2014; Ori-McKenney, Jan, & Jan, 2012; Sanchez-Huertas et al., 2016). In striated (i. e. heart and skeletal) muscle cells, ncMTOCs form at the nuclear envelope and contribute to correct nuclei positioning in skeletal myotubes (Elhanany-Tamir et al., 2012; Espigat-Georger, Dyachuk, Chemin, Emorine, & Merdes, 2016; Gimpel et al., 2017; Kronebusch & Singer, 1987; Tassin, Maro, & Bornens, 1985). Notably, human myopathies, such as centronuclear myopathy (CNM) or Emery-Dreifuss muscular dystrophy (EDMD), often feature mislocalized nuclei (Jungbluth and Gautel, 2014; Madej-Pilarczyk and Kochanski, 2016). While the nuclear envelope MTOC (NE-MTOC) has been implicated

72 in early steps of myonuclear positioning *in vitro*, a direct link between NE-MTOC
73 defects and human myopathies has not been established, possibly due to the fact that
74 many aspects of NE-MTOC formation and function remain unclear. Similarly, while
75 microtubules are important regulators of contractility and nuclear architecture in
76 cardiomyocytes (C. Y. Chen et al., 2018; Heffler et al., 2020), the specific role of NE-
77 MTOC-generated microtubules remains unclear.

78 Despite progress in illuminating identity, composition, and function of ncMTOCs, it
79 remains elusive which mechanisms initiate the switch from centrosomal to non-
80 centrosomal MTOCs during differentiation of vertebrate cells. The only mechanistic
81 insight into ncMTOC induction has been gained by studying *Drosophila* tracheal cells.
82 It was shown that the transcription factor trachealess, which specifies tracheal fate, is
83 required for the spastin-mediated release of centrosomal components from the
84 centrosome and their subsequent Piopio-mediated anchoring to the apical membrane
85 (Brodu et al., 2010).

86 Here, we aimed to identify mechanisms that control NE-MTOC formation in
87 mammals utilizing skeletal muscle differentiation as an experimental system.
88 Mammalian skeletal muscle differentiation is controlled by a family of transcription
89 factors termed myogenic regulatory factors (MRFs) (Braun & Gautel, 2011;
90 Buckingham & Rigby, 2014). Among those, myoblast determination protein (MyoD)
91 regulates commitment to a myogenic fate and is thought to promote early differentiation
92 of myoblasts (Comai & Tajbakhsh, 2014; Ishibashi, Perry, Asakura, & Rudnicki, 2005).
93 The MRF myogenin acts as a unique regulator of terminal differentiation during
94 myogenesis. In the absence of myogenin *in vivo*, embryonic myofiber formation is
95 disturbed and the second wave of fetal myogenesis is largely abolished (Hasty et al.,
96 1993; Nabeshima et al., 1993; Venuti, Morris, Vivian, Olson, & Klein, 1995). Notably,
97 MRFs are able to induce phenotypical markers of skeletal muscle in permissive non-

98 muscle cells (Braun, Bober, Winter, Rosenthal, & Arnold, 1990; Braun, Buschhausen-
99 Denker, Bober, Tannich, & Arnold, 1989; Comai & Tajbakhsh, 2014; Davis, Weintraub,
100 & Lassar, 1987; Edmondson & Olson, 1989; Weintraub et al., 1989). Therefore, we
101 examined whether MRFs regulate NE-MTOC formation during skeletal muscle
102 differentiation and whether they are sufficient for NE-MTOC initiation in non-muscle
103 cells.

104 NE-MTOC formation involves the localization of different MTOC proteins to the
105 nuclear envelope. These include the PCM components pericentrin (PCNT),
106 CDK5RAP2, and AKAP9 (also known as AKAP450) as well as γ-tubulin, key
107 component of γ-tubulin ring complexes (γTuRCs) (Bugnard, Zaal, & Ralston, 2005;
108 Espigat-Georger et al., 2016; Gimpel et al., 2017; Srsen, Fant, Heald, Rabouille, &
109 Merdes, 2009). At the centrosomal MTOC, PCNT, CDK5RAP2, and AKAP9 can
110 interact with and recruit γTuRCs that in turn promote microtubule nucleation (Teixido-
111 Travesa, Roig, & Luders, 2012). At the nuclear envelope of myotubes, microtubule
112 nucleation appears to specifically depend on AKAP9 (Gimpel et al., 2017) and γ-tubulin
113 (Bugnard et al., 2005). Another protein localized to the nuclear envelope is PCM-1, an
114 integral component of centriolar satellites, which contribute to recruiting proteins to the
115 centrosome and proper organization of the centrosomal MTOC (Prosser & Pelletier,
116 2020). In myotubes, PCM-1 is required to recruit microtubule-associated motors to the
117 nuclear envelope (Espigat-Georger et al., 2016).

118 Based on loss and gain of function experiments, quantitative analysis utilizing
119 different cell types, and promoter studies, we show here that myogenin is required and
120 sufficient for the formation of an NE-MTOC by controlling the expression of muscle-
121 and NE-MTOC-specific isoforms of *Akap6* and *Syne1* which encodes nesprin-1α.

Results

Myogenin is required for MTOC protein localization to the nuclear envelope

To gain insight into the regulation of NE-MTOC establishment in skeletal muscle cells, we correlated the expression of MyoD and myogenin during mouse C2C12 myoblast differentiation with two key steps of NE-MTOC formation: 1) The expression of nesprin-1α, the nuclear envelope anchor for MTOC proteins (Espigat-Georger et al., 2016; Gimpel et al., 2017) and 2) the recruitment of PCM-1, the first MTOC protein localizing to the nuclear membrane (Srsen et al., 2009; Zebrowski et al., 2015). Immunofluorescence analyses of C2C12 cells one day after induction of differentiation revealed that 49.1 ± 7% of nuclei were MyoD$^+$, 12 ± 0.9% were myogenin$^+$, 7.8 ± 0.3% were nesprin-1α$^+$, and 1.9 ± 0.3% were PCM-1$^+$ (Figure 1A-C). Note, that intermediate stages of PCM-1 nuclear envelope recruitment can be observed (Figure 1 – figure supplement 1A), suggesting that PCM-1 recruitment occurs in a gradual manner. In our analysis, intermediate stages were rare (<2% of total PCM-1$^+$ nuclei) and have therefore been included in the total percentage of PCM-1$^+$ nuclei.

Prominent MyoD expression was detected in all cells that had upregulated nesprin-1α and recruited PCM1 to the nuclear envelope (Figure 1A-B) suggesting that MyoD-driven early differentiation is required for both steps of NE-MTOC formation. In contrast, the late differentiation factor myogenin was detected in all PCM1$^+$ nuclei (Figure 1B) but only in 42% of nesprin-1$^+$ nuclei (Figure 1A,D). Considering that 1) myogenin is a downstream target of MyoD (Berkes & Tapscott, 2005) and 2) nesprin-1α is anchoring MTOC proteins at the nuclear envelope, this suggested that, during NE-MTOC formation, myogenin might be either dispensable or required for a second step downstream of nesprin-1α.

146 To determine the role of myogenin in MTOC protein localization to the nuclear
147 envelope, we depleted myogenin in C2C12 cells via siRNA and analyzed nesprin-1α
148 expression as well as nuclear envelope localization of the MTOC proteins PCM-1,
149 PCNT, and AKAP9 after two days of differentiation. The number of nesprin-1α$^+$ nuclei
150 was not significantly affected by myogenin depletion (Figure 1E,F). By contrast,
151 knockdown of myogenin reduced the number of PCM-1$^+$ nuclei from 11.6 ± 1.3% in
152 control siRNA-treated cells to 2.3 ± 0.8% (Figure 1E,F) whereby PCM-1 retained a
153 centrosomal localization pattern at highly nesprin-1α$^+$ nuclei in myogenin-depleted
154 cultures (Figure 1 – figure supplement 2), although the pattern was less focused than
155 in undifferentiated myoblasts. Similarly, PCNT$^+$ nuclei were reduced from 6.9 ± 0.1%
156 to 1.4 ± 0.1% and AKAP9$^+$ nuclei showed a reduction from 6.8 ± 0.5% to 1.4 ± 0.1%
157 (Figure 1F and Figure 1 – figure supplement 1B). These data indicate that myogenin
158 is required for MTOC protein localization to the nuclear envelope during skeletal
159 muscle differentiation.

160 Considering that PCM-1 is 1) important for recruitment of other proteins to the
161 centrosome (Dammermann & Merdes, 2002; Prosser & Pelletier, 2020) and 2) the first
162 MTOC protein localizing to the nuclear envelope (Srsen et al., 2009; Zebrowski et al.,
163 2015), we aimed to assess whether the loss of PCM-1 affects the recruitment of other
164 MTOC proteins to the nuclear envelope. Depletion of PCM-1 reduced the percentage
165 of C2C12 nuclei fully or partially positive for PCNT after two days of differentiation from
166 5.8 ± 1% to 0.8 ± 0.2% and 2.7 ± 0.9% to 0.5 ± 0.1%, respectively (Figure 1G,H). In
167 contrast, PCM-1 depletion did not affect recruitment of AKAP9 (Figure 1 – figure
168 supplement 1C). Similar qualitative results have been described in myotubes (Espigat-
169 Georger et al., 2016; Gimpel et al., 2017).

170 Collectively, our data suggest that the myogenin-independent early myogenic
171 differentiation is sufficient to induce nesprin-1α expression, whereas myogenin
172 regulates the nuclear envelope targeting of AKAP9 and PCM-1, which in turn recruits
173 PCNT.
174
175 **Ectopic myogenin expression is sufficient to induce a NE-MTOC**
176 All MRFs are able to "transdifferentiate" permissive non-muscle cells with varying
177 efficiency. They induce skeletal muscle markers such as the expression of contractile
178 proteins or cell fusion into myotubes (Braun et al., 1990; Braun et al., 1989; Davis et
179 al., 1987; Edmondson & Olson, 1989; Weintraub et al., 1989). However, NE-MTOC
180 formation has never been analyzed in "transdifferentiated" cells. To determine whether
181 MRFs are sufficient to induce NE-MTOC formation in non-muscle cells, we ectopically
182 expressed MyoD-GFP, myogenin-GFP or GFP alone in mouse NIH3T3 fibroblasts and
183 analyzed the localization of PCM-1. NIH3T3 cells transfected with GFP exhibited
184 centrosomal PCM-1 localization, typical for proliferating cells (Figure 2A). By contrast,
185 expression of MyoD-GFP and, surprisingly, myogenin-GFP induced nuclear envelope
186 localization of PCM-1 in a subset of GFP^+ cells (Figure 2A,B), suggesting that both
187 MRFs are sufficient individually to induce localization of MTOC proteins to the nuclear
188 envelope.
189 The results obtained upon MyoD-GFP expression are potentially explained by the
190 fact that MyoD is known to activate myogenin transcription (Berkes & Tapscott, 2005).
191 Analyzing endogenous myogenin expression in MyoD-GFP expressing cells, we
192 observed high myogenin levels in cells that had recruited PCM-1 to the nuclear
193 envelope compared to MyoD-GFP expressing cells where PCM-1 was absent from the
194 nuclear envelope (Figure 2 – figure supplement 1A). In addition, depletion of myogenin
195 in NIH3T3 cells abrogated the MyoD-GFP-induced localization of PCM-1 to the nuclear

196 envelope (Figure 2 – figure supplement 1B). To confirm that MyoD regulates the
197 expression of myogenin but not *vice versa*, we analyzed samples of differentiated
198 C2C12 cultures depleted of MyoD or myogenin via RT-PCR (Figure 2 – supplemental
199 figure 1C). While MyoD depletion also reduced myogenin levels, MyoD levels were not
200 detectably affected in myogenin-depleted cultures. Taken together, these results
201 further argue that myogenin is required for the localization of MTOC proteins to the
202 nuclear envelope.

203 In order to elucidate how myogenin – whose expression did not correlate with
204 nesprin-1α in C2C12 cells (Figure 1D) – induces nuclear envelope MTOC formation,
205 we generated stable NIH3T3 cell lines that express either mScarlet or myogenin-2A-
206 mScarlet (MYOG-mScarlet) under control of a tetracycline-responsive promoter (Tet-
207 ON). To induce myogenin expression and, potentially, MTOC protein recruitment to
208 the nuclear envelope, we treated MYOG-mScarlet cells with doxycycline (Dox) for
209 three days. Immunofluorescence analysis revealed that Dox-treatment induced
210 nuclear envelope localization of PCM-1, PCNT, and AKAP9 (Figure 2C, 2E, and 2G).
211 To better account for the dynamic of the recruitment process, we quantified the area
212 of the nuclear envelope positive for each MTOC protein in mScarlet and MYOG-
213 mScarlet cells after Dox treatment (Figure 2D, 2F, and 2H). For this, we set an intensity
214 threshold for the MTOC protein signal and quantified the percentage of pixels above
215 this threshold inside a 1 µm-wide band around the nucleus (identified by DAPI signal).
216 The signal at the centrosome, which localizes in close proximity to the nucleus in most
217 cells, accounts for the nuclear envelope coverage in mScarlet cells. Quantification
218 revealed that median PCM-1 nuclear envelope coverage increases from 12.5% in
219 mScarlet cells to 30.3% in MYOG-mScarlet cells (Figure 2D). PCNT was recruited with
220 an increase of the median coverage from 8.2% in mScarlet cells to 23.1% in MYOG-
221 mScarlet cells (Figure 2F). AKAP9, which is essential for microtubule nucleation at the

222 nuclear envelope (Gimpel et al., 2017), coverage increased only moderately from 3.6%
223 to 6.2%, suggesting that AKAP9 recruitment is less efficient in MYOG-mScarlet cells
224 compared to PCM-1 and PCNT (Figure 2H). However, ~13% of analyzed MYOG-
225 mScarlet nuclei showed a higher coverage than the maximum observed in mScarlet-
226 cells. Together, these data indicate that myogenin is sufficient to induce nuclear
227 envelope localization of MTOC proteins in non-muscle cells.

228 As nuclear envelope localization of MTOC proteins requires nesprin-1α in C2C12
229 cells (Espigat-Georger et al., 2016; Gimpel et al., 2017), we examined whether
230 myogenin is able to induce nesprin-1α expression in Dox-treated MYOG-mScarlet
231 cells. Dox-treatment resulted in nesprin-1^{+} nuclei (Figure 2I) and RT-PCR analysis
232 confirmed that the α-isoform of nesprin-1 is upregulated upon myogenin induction
233 (Figure 2J). This indicate that myogenin can induce nesprin-1α expression. Notably,
234 chromatin immunoprecipitation (ChIP) sequencing data available through the
235 ENCODE consortium (Consortium et al., 2020; Yue et al., 2014) predict myogenin as
236 well as MyoD to bind a candidate regulatory element in the *Syne1* gene near the
237 transcription start site of the nesprin-1α isoform. To examine whether myogenin directly
238 induces nesprin-1α transcription in MYOG-mScarlet cells by binding to the α-isoform-
239 specific promoter in *Syne1*, we performed ChIP, using an anti-myogenin antibody and
240 an isotype control, followed by PCR for the ENCODE-predicted site. PCR amplification
241 was successful from myogenin-precipitated DNA but not from IgG1 control (Figure 2K),
242 indicating that myogenin binds the nesprin-1α promoter. To further substantiate these
243 results, we probed lysates of Dox-treated mScarlet cells and MYOG-mScarlet cells
244 maintained in Dox-free medium. Under both conditions, myogenin expression is not
245 detectable. Additionally, we included an intronic region of *Syne1* as negative control
246 as well as a promoter region of the known myogenin target *Des* (desmin) (Londhe &
247 Davie, 2011) as positive control (Figure 2 – supplemental figure 2). Analysis revealed

248 that the nesprin-1α promoter as well as the desmin promoter were precipitated using
249 the myogenin antibody only in Dox-treated MYOG-mScarlet cells. Therefore, we
250 conclude that myogenin binds the nesprin-1α promoter in *Syne1* and can induce
251 expression of nesprin-1α in permissive cells.

252 Finally, we examined if the myogenin-induced recruitment of MTOC proteins
253 converts the nuclear envelope to a functional MTOC. For this we analyzed microtubule
254 regrowth after cold-induced depolymerization in Dox-treated mScarlet and MYOG-
255 mScarlet cells (Figure 2L and Figure 2 – Figure supplement 3). In mScarlet-expressing
256 cells, microtubule regrowth was observed from the centrosome. In contrast, MYOG-
257 mScarlet cells exhibited microtubule regrowth from the nuclear envelope to varying
258 degrees. Quantification revealed that median nuclear envelope coverage increased
259 from 10.1% in mScarlet cells to 18.4% in MYOG-mScarlet cells.

260 Collectively, these data demonstrate that myogenin is sufficient to induce NE-
261 MTOC formation in NIH3T3 fibroblasts.

262

263 **Myogenin expression attenuates the centrosomal MTOC**

264 In different cell types, it has been observed that ncMTOC formation is associated with
265 attenuation of the centrosomal MTOC (Leask, Obrietan, & Stearns, 1997; Muroyama,
266 Seldin, & Lechler, 2016; Nguyen, Stone, & Rolls, 2011; Yang & Feldman, 2015;
267 Zebrowski et al., 2015). Therefore, we examined if myogenin expression induces
268 centrosome attenuation in MYOG-mScarlet fibroblasts. Dox stimulation resulted in a
269 significant reduction of PCNT levels at centrioles in MYOG-mScarlet cells when
270 compared to Dox-treated mScarlet cells (Figure 3A,B). In contrast, levels of Cep135,
271 a centriole-associated protein, which does not relocalize to the nuclear envelope in
272 muscle cells, did not change significantly upon myogenin induction (Figure 3C,D)
273 indicating that myogenin affects centrosomal localization of PCM proteins but not of

274 centriole-associated proteins. To test if myogenin attenuates MTOC activity at the
275 centrosome, we analyzed centrosomal levels of the microtubule nucleating factor γ-
276 tubulin. Induced MYOG-mScarlet cells displayed a significant reduction in centrosomal
277 γ-tubulin levels compared to mScarlet control cells (Figure 3E). Analyzing microtubule
278 regrowth, we observed that centrosomes still nucleated microtubules in MYOG-
279 mScarlet cells that exhibited microtubule nucleation at the nuclear envelope (Figure
280 3F). However, α-tubulin signal at centrioles was less intense in MYOG-mScarlet cells
281 compared to mScarlet cells, indicating a reduced MTOC activity (Figure 3F). Taken
282 together, these data indicate that myogenin expression – in parallel to inducing
283 ncMTOC formation – attenuates the centrosomal MTOC and that centrosomal and NE-
284 MTOC can be active at the same time.
285

286 **AKAP6 is a potential mediator of myogenin-induced NE-MTOC formation**

287 The myogenin depletion experiments suggested that the sole presence of nesprin-1α
288 at the nuclear envelope does not allow efficient recruitment of MTOC components
289 during muscle differentiation (Figure 1F). Thus, myogenin potentially contributes to the
290 recruitment process by controlling the expression of proteins that are necessary for
291 1) inhibiting the localization of MTOC proteins to the centrosome, 2) targeting MTOC
292 proteins to the nucleus, and/or 3) anchoring MTOC proteins to the nuclear envelope
293 via nesprin-1α.

294 In order to identify candidates that act downstream of myogenin and mediate NE-
295 MTOC formation, we integrated published myogenin ChIP-Seq data (Yue et al., 2014)
296 with RNA-Seq data of C2C12 differentiation (Doynova, Markworth, Cameron-Smith,
297 Vickers, & O'Sullivan, 2017) (Figure 4A). Myogenin ChIP-Seq data was obtained at
298 four different time points (myoblasts, 24 h differentiation, 60 h differentiation, and 7
299 days differentiation; see Methods section for details) whereas the RNA-Seq data-set

300 contained three time points (myoblasts as well as differentiating C2C12 cells at 3 days
301 and 7 days of differentiation). PCM-1 nuclear envelope localization can already be
302 observed 24 h after induction of differentiation (Figure 1A), but the number of cells
303 which differentiate and form an NE-MTOC significantly increases over time.
304 Additionally, we assumed genes required for the maintenance of the NE-MTOC in
305 differentiated cells have to be actively transcribed. Therefore, we considered only
306 those myogenin binding sites in our analysis which were detected in the ChIP-Seq
307 data-set at 24 h, 60 h, and 7 days of differentiation. The promoters of 2462 genes were
308 bound by myogenin at these three time points (Figure 4B). We then intersected these
309 2462 genes with a list of 3800 genes, which were upregulated in the RNA-Seq data-
310 set at both 3 days and 7 days of differentiation when compared to proliferating
311 myoblasts (Figure 4B). This intersection yielded a list of 748 potential direct myogenin
312 target genes (Figure 4B). Considering that skeletal muscle cells and cardiomyocytes
313 (myogenin-negative) both express nesprin-1α and exhibit an NE-MTOC, we
314 hypothesized that NE-MTOC formation in both cell types is controlled by similar
315 mechanisms. Thus, we assessed whether any of the 748 target genes are upregulated
316 during rat heart development from embryonic day 15 to postnatal day 3, the
317 developmental window in which NE-MTOCs form in cardiomyocytes (Zebrowski et al.,
318 2015). For this purpose, we utilized a microarray-derived temporal expression data-set
319 spanning rat heart development (Patra et al., 2011). This strategy helped to further
320 reduce the number of candidate genes to 107 myogenin targets that potentially
321 mediate NE-MTOC formation (Supplementary file 1). As our previous data suggested
322 that nesprin-1α alone does not allow efficient recruitment of MTOC proteins to the
323 nuclear envelope, we first focused on candidates that potentially cooperate with
324 nesprin-1α in anchoring MTOC proteins to the nuclear envelope. To this end, we
325 utilized Gene Ontology analysis to identify candidates that are annotated to localize at

326 the nuclear envelope (Figure 4A). Four genes matched the Gene Ontology cellular
327 component search terms “nuclear membrane” and “nuclear envelope”: *Akap6*, *Dmpk*,
328 *Rb1cc1*, and *Tmem38a*. Previous studies indicated that myogenin directly binds and
329 activates the promoter of *Akap6* (S. W. Lee et al., 2015), which encodes the large
330 scaffold A-kinase anchoring protein (AKAP) 6 (also known as mAKAP). AKAP6 has
331 been described to localize to the nuclear envelope of cardiomyocytes through
332 interaction with the N-terminal spectrin domains of nesprin-1α and to act as a signaling
333 hub by assembling signaling proteins such as protein kinase A, ryanodine receptor,
334 phosphodiesterase 4D3 and phospholipase C (Kapiloff, Schillace, Westphal, & Scott,
335 1999; Pare, Easlick, Mislow, McNally, & Kapiloff, 2005; Passariello, Li, Dodge-Kafka,
336 & Kapiloff, 2015; Ruehr et al., 2003). Furthermore, proximity labeling indicated that
337 AKAP6 is an interactor of nesprin-1α in C2C12 myotubes (Gimpel et al., 2017). Taken
338 together, these data identify AKAP6 as a potential mediator of myogenin-induced NE-
339 MTOC formation.

340 AKAP6 occurs in two isoforms: The brain-specific α-isoform and the β-isoform,
341 which is predominantly expressed in heart and skeletal muscle (Michel et al., 2005).
342 We first determined if myogenin binds the β-isoform promoter of *Akap6* in MYOG-
343 mScarlet fibroblasts and if AKAP6β expression is induced in these cells upon Dox
344 treatment. We could amplify an E-Box containing region of the β-isoform promoter after
345 ChIP using an anti-myogenin antibody (Figure 4C). This result was confirmed by qPCR
346 analysis of the ChIP samples revealing that the Akap6β promoter region is specifically
347 enriched after precipitation with the myogenin antibody in Dox-treated MYOG-mScarlet
348 samples but not in Dox-treated mScarlet or untreated MYOG-mScarlet samples
349 (Figure 4 – supplemental figure 1). Consistently, RT-PCR analysis showed that
350 AKAP6β is upregulated after Dox stimulation (Figure 4D). Collectively, these data

351 indicate that, in fibroblasts, myogenin can bind the *Akap6*β-isoform promoter and
352 induce AKAP6 expression.

353 To determine whether nesprin-1α is – similar to the situation in cardiomyocytes –
354 involved in AKAP6β localization to the nuclear envelope of skeletal muscle cells (Pare
355 et al., 2005), we analyzed the expression pattern of AKAP6 (refers to the β isoform if
356 not specified) and nesprin-1α in C2C12 cells. Immunofluorescence analysis at two
357 days differentiation showed that all AKAP6$^+$ nuclei were nesprin-1α$^+$ (Figure 4E). In
358 addition, high-resolution microscopy suggested that AKAP6 mainly localizes at the
359 cytoplasmic side of nesprin-1α (Figure 4F and Figure 4 – figure supplement 2). It has
360 been reported that the C-terminus of nesprin-1α is inserted into the outer nuclear
361 membrane, whereas the N-terminus extends into the cytoplasm (Apel, Lewis, Grady,
362 & Sanes, 2000; Q. Zhang et al., 2001).

363 To test if nesprin-1α is required to anchor AKAP6 to the nuclear envelope, patient-
364 derived myoblasts carrying a mutation in the *SYNE1* gene (23560 G>T causing a
365 premature stop and loss nesprin-1α expression) and myoblasts of healthy donors were
366 differentiated into myotubes and AKAP6 localization was compared (Figure 4G).
367 Whereas nesprin-1α and AKAP6 localized to the nuclear envelope of myotubes from
368 healthy donors, expression of nesprin-1α and nuclear membrane localization of AKAP6
369 were abolished in myotubes carrying the *SYNE1* mutation. Taken together, these data
370 indicate that AKAP6 localization to the nuclear envelope in differentiated skeletal
371 muscle cells depends on nesprin-1α.

372

373 **AKAP6 is required for NE-MTOC formation and maintenance**

374 To examine the role of AKAP6 in NE-MTOC formation we performed siRNA-mediated
375 depletion experiments in differentiating C2C12 cells and MYOG-mScarlet fibroblasts.
376 In C2C12 cultures differentiated for two days, 12.3 ± 0.6% of nuclei were AKAP6$^+$ and

377 10.4 ± 1.2% of nuclei were PCM-1$^+$ (Figure 5A,B). Importantly, AKAP6 was found at
378 all nuclei that had recruited PCM-1. Transfection of differentiating C2C12 cultures with
379 AKAP6 siRNA significantly reduced the number of AKAP6$^+$ nuclei from 12.3 ± 0.6% to
380 4.8 ± 0.1% and the number of PCM-1$^+$ nuclei from 10.4 ± 1.2% to 3.4 ± 0.3% (Figure
381 5B) but had no effect on nesprin-1α localization (Figure 5 - figure supplement 1).
382 Correspondingly, treatment of Dox-induced MYOG-mScarlet with AKAP6 siRNA
383 decreased median nuclear envelope coverage by PCM-1 and PCNT from 22.6% to
384 9% and 18.7% to 5.5%, respectively (Figure 5C-E). Median coverage of AKAP9 was
385 only moderately affected (7.2% to 6.5%) but nuclei showing more than ~18% AKAP9
386 coverage were completely lost after AKAP6 depletion (Figure 5F). To examine if
387 AKAP6 promotes nuclear envelope recruitment by forming a complex with MTOC
388 proteins, we performed co-immunoprecipitation experiments using an anti-AKAP6
389 antibody. We could co-precipitate PCM-1 from MYOG-mScarlet lysates but not from
390 mScarlet lysate (Figure 5G). These data indicate that AKAP6 is required for the
391 localization of MTOC proteins to the nuclear envelope, in part by forming a protein
392 complex including PCM-1.

393 To examine whether the recruitment of MTOC proteins to the nuclear envelope is
394 the reason for the attenuation of the centrosomal MTOC in MYOG-mScarlet
395 fibroblasts, we analyzed centrosomal levels of PCNT and γ-tubulin in AKAP6-depleted
396 or nesprin-1α-depleted cells (Figure 5 – figure supplement 2). We did not observe an
397 increase of centrosomal PCNT or γ-tubulin levels in AKAP6- or nesprin-1-depleted
398 cultures, indicating that the main mechanism for centrosome attenuation is not the
399 competition with the NE-MTOC.

400 To determine if AKAP6 is required for maintaining MTOC protein localization at the
401 nuclear envelope, we transfected C2C12 cultures enriched for myotubes with AKAP6

402 siRNA (Figure 5H, I). Depletion of AKAP6 resulted in the loss of PCM-1, AKAP9, and
403 PCNT from the nuclear envelope in myotubes.
404 Taken together, our data demonstrate that AKAP6 is required for recruiting MTOC
405 proteins to the nuclear envelope as well as maintaining nuclear envelope localization
406 of MTOC proteins in myotubes, most likely by acting as an adaptor between MTOC
407 proteins and the nuclear membrane anchor nesprin-1α.
408
409 **MyoD can induce AKAP6 expression via myogenin**
410 Similar to myogenin, ectopic expression of MyoD was sufficient to induce PCM-1
411 localization to the nuclear envelope (Figure 2A, B). Consistently, a more detailed
412 analysis of MyoD-GFP-transfected NIH3T3 cells revealed that nesprin-1 and AKAP6
413 expression is induced in these cells as well (Figure 5 – supplemental figure 3). As
414 previous depletion experiments indicated that MyoD induces PCM-1 localization to the
415 nuclear envelope via myogenin (Figure 2 – supplemental figure 1), we analyzed
416 nesprin-1 and AKAP6 in MyoD-GFP-transfected cells treated with myogenin siRNA.
417 Analysis revealed that the percentage of nesprin-1^{+} nuclei in GFP^{+} cells was not
418 affected by myogenin depletion (Figure 5 – supplemental figure 3), which is consistent
419 with our findings in C2C12 cells (Figure 1F). However, the percentage of AKAP6^{+} as
420 well as PCM-1^{+} nuclei was reduced upon myogenin depletion. This further shows that
421 MyoD-induced MTOC protein localization to the nuclear envelope depends on the
422 induction of myogenin.
423
424 **AKAP6 is required for NE-MTOC function**
425 The NE-MTOC has been described to be required for correct positioning and
426 distribution of nuclei in multinucleated myotubes via two different mechanisms: 1)
427 PCM-1 enables the recruitment of the dynein regulator p150glued and other motor

428 proteins to the nuclear envelope and promotes alignment of nuclei (Espigat-Georger
429 et al., 2016), and 2) Akap9-dependent nucleation of microtubules from the nuclear
430 envelope contributes to the spreading of nuclei throughout the cell body (Gimpel et al.,
431 2017) (Figure 6A). Our results indicate a potential role for AKAP6 in both aspects of
432 nucleus positioning as it is required for PCM-1 and AKAP9 to localize to the nuclear
433 envelope. Analyzing the positioning and distribution of nuclei in enriched C2C12
434 myotubes two days after siRNA-mediated depletion of AKAP6, we found that AKAP6
435 depletion reduced the number of myotubes with aligned nuclei (66.0 ± 7.5% to 34.7 ±
436 7.6%) and increased the number of myotubes with overlapping nuclei (26.0 ± 6.5% to
437 58.3 ± 9.6%), compared to control myotubes (Figure 6B,C). This indicates that AKAP6
438 is required for proper alignment and spreading of nuclei in myotubes.

439 Next, we aimed to confirm that the observed nuclei mispositioning in AKAP6-
440 depleted cells is due to aberrant microtubule nucleation and motor protein recruitment
441 at the nuclear envelope. Immunofluorescence analysis showed that two days post
442 siRNA transfection the microtubule network organization was similar in AKAP6-
443 depleted and control myotubes showing the typical organization of microtubules in
444 longitudinal arrays (Figure 6 – figure supplement 1A). Similar results have been
445 obtained previously when depleting nesprin-1α (Espigat-Georger et al., 2016). Yet, we
446 observed that AKAP6 depletion resulted in a reduced intensity of detyrosinated (i.e.
447 stable) microtubules compared to control myotubes (Figure 6 – figure supplement 1B).
448 To test if AKAP6 depletion affects the nucleation of new microtubules, we assessed
449 microtubule regrowth after nocodazole-induced depolymerization in C2C12 myotubes.
450 In myotubes treated with control siRNA, microtubules regrew from the nuclear
451 envelope and to a lesser extent from cytoplasmic loci (Figure 6D). In AKAP6-depleted
452 myotubes, microtubule regrowth from the nuclear envelope was abolished (Figure 6D).
453 This suggests that AKA6 depletion impairs spreading of myonuclei by preventing

454 microtubule growth from the nuclear envelope. Next, we analyzed the localization of
455 p150glued (also known as DCTN1). In control siRNA-treated myotubes, p150glued
456 localized at the nuclear envelope (Figure 6E). AKAP6 depletion resulted in a reduction
457 of p150glued at the nuclear envelope of C2C12 myotubes (Figure 6E) suggesting that
458 the reduced number of myotubes with aligned nuclei is due to impaired dynein
459 activation. Collectively, these data demonstrate that AKAP6 is required for the function
460 of the NE-MTOC in skeletal muscle cells.
461

462 **Myogenin-induced isoforms of nesprin-1 and AKAP6 are sufficient for MTOC**
463 **protein recruitment**

464 To examine if myogenin specifically induces expression of isoforms that are associated
465 with the NE-MTOC in skeletal muscle, we performed ChIP on MYOG-mScarlet cell
466 lysate using an anti-myogenin antibody and assessed the abundance of isoform-
467 specific promoter regions of *Syne1* and *Akap6* in the precipitated DNA. For this, we
468 performed semi-quantitative PCR (qPCR) using primer pairs targeting myogenin
469 consensus binding sites (i.e. E-boxes) in regions predicted by ENCODE data
470 (Consortium et al., 2020) to be associated with myogenin binding (Figure 7A,C). We
471 found that the amount of template corresponding to the promoter region upstream of
472 the nesprin-1α transcript (nesprin-1α2) was 4.5-fold higher than the promoter region of
473 the long nesprin-1 isoform (nesprin-1-giant) (Figure 7B). Similarly, the promoter region
474 upstream of the AKAP6β transcript was 3-fold enriched compared to the promoter
475 region of the AKAP6α transcript (Figure 7D). This indicates that myogenin
476 preferentially binds promoter regions of *Syne1* and *Akap6* isoforms that are involved
477 in NE-MTOC formation.

478 To test if the preferential binding is associated with an increased activation of
479 transcription of specific isoforms, we constructed vectors with putative promoter

480 regions of AKAP6α, AKAP6β, nesprin-1-giant, or nesprin-1α located directly upstream
481 of a luciferase coding sequence and transfected them into human HEK293T cells
482 together with GFP or myogenin-GFP. Co-transfection of myogenin with the AKAP6β
483 promoter construct increased luciferase activity 10.9-fold, while co-transfection with
484 the AKAP6α promoter construct did not show a significant increase compared to GFP-
485 transfected control (Figure 7E). Similarly, we observed a 21.7-fold increase in activity
486 when myogenin was co-transfected with the nesprin-1α promoter construct but only a
487 mild 2.7-fold increase after co-transfection with the promoter construct of nesprin-1-
488 giant (Figure 7F). These results indicate that myogenin preferentially induces
489 transcription of nesprin-1α and AKAP6β.

490 Finally, we examined whether the myogenin-induced isoforms of nesprin-1 and
491 AKAP6 are sufficient to recruit MTOC proteins in the absence of myogenin. For this,
492 we expressed nesprin-1α-mCherry alone or together with AKAP6β-GFP in
493 undifferentiated, myogenin-negative myoblasts. In nesprin-1α-mCherry-transfected
494 cells, PCM-1 did not localize to the nuclear envelope (Figure 7G). In contrast, co-
495 transfection of nesprin-1α-mCherry and AKAP6β-GFP was sufficient to recruit PCM-1
496 to the nuclear envelope (Figure 7G). To test whether co-expression of nesprin-1α and
497 AKAP6β is sufficient to convert the nuclear envelope to a functional MTOC, we
498 performed microtubule regrowth experiments (Figure 7 – supplemental figure 1).
499 Microtubules regrew from the centrosome and in the cytoplasm, but significant
500 regrowth from the nuclear envelope was not observed.

501 Taken together, our results demonstrate that myogenin specifically induces
502 transcription of isoforms which are 1) required for the NE-MTOC in differentiated
503 skeletal muscle cells and 2) sufficient to recruit MTOC proteins to the nuclear envelope
504 in cells with a centrosomal MTOC.

505

506 **Discussion**

507 We conclude that the myogenic transcription factor myogenin controls NE-MTOC
508 formation and that myogenin-induced AKAP6β expression is one of the central
509 molecular components required for NE-MTOC formation (Figure 8). This conclusion is
510 supported by our findings that 1) myogenin is required for the localization of the MTOC
511 proteins PCM-1, PCNT and AKAP9 to the nuclear envelope in differentiating muscle
512 cells, 2) ectopic myogenin expression is sufficient to promote the formation of an NE-
513 MTOC in fibroblasts, and 3) the myogenin-induced isoforms AKAP6β and nesprin-1α
514 are required and sufficient for the recruitment of MTOC proteins to the nuclear
515 envelope.

516 Formation of ncMTOCs has been associated with cellular differentiation (Sanchez
517 & Feldman, 2017), but a direct regulation of ncMTOC formation by particular
518 differentiation pathways in vertebrate cells has remained elusive. Our results
519 demonstrate that myogenin, which is an essential regulator of terminal differentiation,
520 drives NE-MTOC formation in mammalian cells. This shows that terminal differentiation
521 factors can control in vertebrates the switch of dominant MTOC localization from the
522 centrosome to non-centrosomal sites. Notably, MTOC formation at the nuclear
523 envelope occurs also in cells that lack myogenin or cell-type specific transcriptional
524 master regulators of terminal differentiation, such as cardiomyocytes or osteoclasts
525 (Kronebusch & Singer, 1987; Mulari et al., 2003; Zebrowski et al., 2015). A recent study
526 from our lab demonstrated that AKAP6β orchestrates the assembly of the NE-MTOC
527 in cardiomyocytes and osteoclasts (Vergarajauregui et al., 2020), validating our
528 findings in skeletal muscle. Therefore, it would be important in future studies to identify
529 transcription factors that bind to AKAP6β and nesprin-1α promoters and regulate the
530 switch from centrosomal to NE-MTOC in these cell types. For this purpose, promising
531 cardiomyocyte and osteoclast “transdifferentiation” tools using multiple transcription

532 factors are available (Chang, Cho, Kim, & Kim, 2019; Ieda et al., 2010; Klose, Gossen,
533 & Stamm, 2019; Yamamoto et al., 2015). Additionally, it appears important to
534 determine in future experiments the mechanisms underlying the preferential binding of
535 myogenin to the isoform-specific promoters, considering the abundance of myogenin
536 binding sites (E-boxes) throughout the genome. Notably, isoform upregulation or
537 switching might be a general mechanism that contributes to MTOC regulation during
538 differentiation. This assumption is supported by the recent identification of a spermatid-
539 specific isoform of centrosomin, the *Drosophila* orthologue of CDK5RAP2, which can
540 induce ncMTOC formation at mitochondria (J. V. Chen, Buchwalter, Kao, & Megraw,
541 2017). Moreover, a non-centrosomal isoform of ninein contributes to neuronal
542 differentiation (X. Zhang et al., 2016) and a shorter isoform of PCNT is upregulated in
543 differentiating cardiomyocytes (Zebrowski et al., 2015).

544 Both MyoD and myogenin induced expression of nesprin-1α and AKAP6 as well
545 as the nuclear envelope localization of PCM-1. The depletion experiments in
546 differentiating C2C12 cells and in MyoD-transfected fibroblasts indicate that myogenin
547 is required for the localization of MTOC proteins to the nuclear envelope via AKAP6
548 expression. While myogenin can induce nesprin-1α expression in fibroblasts, it is
549 dispensable for nesprin-1α upregulation during C2C12 differentiation. Together, these
550 findings suggest a model of NE-MTOC formation during C2C12 differentiation in which
551 MyoD induces nesprin-1α as well as myogenin, which is then required to induce
552 AKAP6 expression allowing recruitment of MTOC proteins to the nuclear envelope.

553 The centrosomal MTOC is attenuated in differentiated muscle cells (Becker,
554 Leone, & Engel, 2020). Consistently, we found that ectopic myogenin expression in
555 fibroblasts resulted in reduced MTOC protein levels at centrosomes as well as
556 attenuated centrosomal microtubule regrowth. Depletion of nesprin-1α or AKAP6 in
557 this system – abolishing the localization of MTOC proteins to the nuclear envelope –

558 did not result in obvious reactivation of the centrosomal MTOC, indicating that
559 centrosome attenuation is not due to competition with the NE-MTOC. Furthermore,
560 differentiating C2C12 cells in which myogenin was depleted maintained PCM-1 in a
561 centriolar satellite-like pattern, albeit this pattern was less focused. Taken together,
562 these results suggest that myogenin attenuates the centrosome during muscle
563 differentiation independently of inducing NE-MTOC formation.

564 While site-specific anchor proteins for ncMTOCs, such as nesprin-1α, have been
565 identified (Espigat-Georger et al., 2016; Gimpel et al., 2017; Lechler & Fuchs, 2007;
566 Meng, Mushika, Ichii, & Takeichi, 2008), it remained unclear how MTOC proteins are
567 connected to these site-specific anchors. Previously, it has been reported that
568 overexpression of nesprin-1α in undifferentiated myoblasts is sufficient to recruit an
569 ectopically expressed centrosomal targeting domain of PCNT and AKAP9 (i.e. the
570 PACT domain) as well as minor amounts of endogenous PCM-1 to the nuclear
571 envelope in a subset of transfected cells (Espigat-Georger et al., 2016; Gimpel et al.,
572 2017). Here, we show that myogenin induced the expression of the large scaffold
573 protein AKAP6, which we prove to be essential for NE-MTOC formation and
574 maintenance, most likely by connecting MTOC proteins to nesprin-1α. Myogenin
575 preferentially binds and activates the putative promoters of AKAP6β and nesprin-1α
576 isoforms, which are known to be upregulated in differentiated muscle cells (Kapiloff et
577 al., 1999; Michel et al., 2005; Randles et al., 2010). Importantly, ectopic co-expression
578 of AKAP6β and nesprin-1α, but not nesprin-1α alone, was sufficient to recruit
579 endogenous MTOC proteins in the absence of myogenin.

580 Our results indicate an important role of AKAP6-dependent NE-MTOC function in
581 nucleus positioning in skeletal myotubes *in vitro*. While nucleus positioning is a
582 frequent feature of human myopathies (Jungbluth and Gautel, 2014; Madej-Pilarczyk
583 and Kochanski, 2016), the specific role of the NE-MTOC in these pathologies remains

584 largely elusive. Yet, mutations in the nesprin-1 gene *SYNE1* have been described in
585 EDMD patients, pointing towards a potential role of NE-MTOC defects in this pathology
586 (Zhang et al., 2007). Fully elucidating the mechanisms of NE-MTOC formation *in vivo*
587 and the specific contributions of nuclear envelope-originated microtubules to the
588 different aspects of myonuclear positioning will clarify if and how NE-MTOC defects
589 contribute to human myopathies. In addition to nucleus positioning, microtubules help
590 to maintain nuclear architecture in myotubes (Wang, Reuveny, & Volk, 2015) and
591 cardiomyocytes (Heffler et al., 2020) and also regulate contractility (C. Y. Chen et al.,
592 2018). While perinuclear microtubules have been identified to be specifically important
593 for nuclear architecture, the significance of the NE-MTOC in this context remains
594 unclear. Precise targeting of the NE-MTOC via AKAP6 appears a promising strategy
595 to elucidate the role of nuclear envelope-generated microtubules in maintaining
596 nuclear architecture as well as regulating contractility. Finally, amplified and/or
597 hyperactive centrosomes act as oncogene-like factors (Arnandis et al., 2018; Godinho
598 & Pellman, 2014; Godinho et al., 2014; Levine et al., 2017; LoMastro & Holland, 2019).
599 Therefore, it is important to better understand mechanisms that control MTOC activity.
600 Notably, ectopic expression of myogenin in fibroblasts did not only induce NE-MTOC
601 formation but also attenuated the centrosomal MTOC. In addition, myogenin
602 expression in fibroblast was only inducing in a subset of cells an NE-MTOC. Thus, our
603 cellular systems combined with our bioinformatics approach provides new
604 opportunities to tackle future key questions of MTOC formation such as: What factors
605 increase or decrease efficiency of NE-MTOC induction? What post-transcriptional
606 processes contribute to NE-MTOC establishment? How is centrosome attenuation
607 achieved?

608 In summary, our findings suggest that key differentiation factors can control the
609 switch from centrosomal MTOC to ncMTOC and cell-type specific adaptor proteins are

610 required to connect MTOC proteins to anchor proteins at non-centrosomal sites.
611 Conclusively, our study 1) contributes to a better understanding of the striated muscle
612 NE-MTOC, 2) presents a mechanistic framework that may be applicable to ncMTOC
613 formation in other cell types and tissues, and 3) provides a cellular system to elucidate
614 further molecular mechanisms inducing the switch from centrosomal to ncMTOCs.

615 **Material and Methods**

616 Further information and requests for resources and reagents should be directed to and
617 will be fulfilled by the lead contact, Felix Engel (felix.engel@uk-erlangen.de).

618

619 **Cell lines, differentiation and doxycycline stimulation**

620 The following cell lines have been used in the present study:

Cell Lines	Source	Catalogue number/ Identifier
Mouse: C2C12 myoblast cell line	ATCC	Cat# CRL-1772, RRID: CVCL_0188
Mouse: NIH3T3 fibroblast cell line	ATCC	Cat# CRL-1658, RRID:CVCL_0594
Human: HEK293T cell line	ATCC	Cat# PTA-4488, RRID:CVCL_0045
Human: myoblasts healthy donor	(Holt et al., 2016; Mamchaoui et al., 2011)	N/A
Human: myoblasts carrying SYNE1 mutation	(Holt et al., 2016; Mamchaoui et al., 2011)	N/A

621

622 Cell types were authenticated as follows: human myoblasts and C2C12, myotube
623 formation; NIH3T3, morphology; HEK293, efficiency in protein production. Note,
624 identity of NIH3T3 and HEK293T cells is not essential for this study. All cell lines were
625 mycoplasma-free (tested every 12 months).

626 Reagents used for cell culture are listed in the table below. All cells used in this
627 study were cultured at 37°C in a humidified atmosphere containing 5% CO_2. Growth
628 medium for C2C12, NIH3T3, Hela and Hct116 consisted of high glucose DMEM
629 supplemented with GlutaMAX containing 10% FBS, 1 mM sodium pyruvate, 100 U/ml
630 penicillin and 100 µg/ml streptomycin. C2C12 cells were maintained at 50% confluence
631 to preserve differentiation capacity. For differentiation, cells were cultured to 90%

632 confluence and subsequently changed to differentiation medium (high glucose DMEM
633 with GlutaMAX containing 0.5% FBS and Insulin, Transferrin, Selenium, Sodium
634 Pyruvate Solution (1:1000 of 100x ITS-A).

635 Human myoblasts from a healthy control or from a congenital muscular dystrophy
636 patient carrying a homozygous nonsense mutation within the *SYNE1* gene (nucleotide
637 23560 G>T) were immortalized by Kamel Mamchaoui and Vincent Mouly (Center for
638 Research in Myology, Paris, France) as previously described via transduction with
639 retrovirus vectors expressing hTERT and Cdk4 (Holt et al., 2016; Mamchaoui et al.,
640 2011). Growth medium consisted of DMEM supplemented with GlutaMAX and DMEM
641 199 in a 4:1 ratio containing 20% FBS, 25 µg/ml bovine fetuin, 5 ng/ml recombinant
642 human EGF, 0.5 mg/ml recombinant human FGF-basic, 5 µg/ml recombinant insulin,
643 0.2 µg/ml dexamethasone, and 50 µg/ml gentamicin (Gimpel et al., 2017). To induce
644 differentiation, immortalized myoblasts were grown to ~90% confluence and then
645 changed to Skeletal Muscle Differentiation Medium (PromoCell) containing 50 µg/ml
646 gentamicin. For immunofluorescence analysis of immortalized myoblasts, glass
647 coverslips were coated with Matrigel diluted 1:100 in DMEM.

Cell culture reagent	Source	Catalogue number/ Identifier
0.25% Trypsin/EDTA solution	Sigma Aldrich	Cat# T4049
Dulbecco's Modified Eagle Medium (DMEM), high glucose, GlutaMAX	Thermo Fisher Scientific	Cat# 61965059
DMEM 199 medium	Thermo Fisher Scientific	Cat# 41150
Skeletal Muscle Differentiation Medium	PromoCell	Cat# C-23061
Fetal Bovine Serum (FBS)	biowest	Cat# S1810
Fetal Bovine Serum (FBS), tetracycline free	PAN-Biotech	Cat# P30-3602
Doxycycline hydrochloride	Sigma-Aldrich	Cat# D3447
Horse Serum	Thermo Fisher Scientific	Cat# 16050122
Sodium pyruvate solution	Sigma-Aldrich	Cat# S8636

Penicillin-Streptomycin	Thermo Fisher Scientific	Cat# 15140122
Gentamicin	Thermo Fisher Scientific	Cat# 15750060
Insulin-Transferrin-Selenium-Sodium Pyruvate (ITS-A) (100X)	Thermo Fisher Scientific	Cat# 51300044
Bovine fetuin	Thermo Fisher Scientific	Cat# 10344026
EGF Recombinant Human Protein	Thermo Fisher Scientific	Cat# PHG0311
FGF-Basic (AA 10-155) Recombinant Human Protein	Thermo Fisher Scientific	Cat# PHG0026
Insulin, Human Recombinant	Sigma-Aldrich	Cat# 91077C
Dexamethasone	Sigma-Aldrich	Cat# D4902
Matrigel® hESC-Qualified Matrix, LDEV-free	Corning	Cat# 356277
Fibronectin bovine plasma	Sigma-Aldrich	Cat# F1141

648

649 **Myotube enrichment**

650 C2C12 cells were differentiated in 6-well plates or 10 cm dishes for 4-5 days as
651 described above. To preferentially detach myotubes, cells were washed two times with
652 PBS and treated with pre-warmed 0.0125% Trypsin/EDTA solution (0.25%
653 Trypsin/EDTA stock diluted in PBS) for ~2 min at room temperature. Detachment of
654 myotubes was constantly monitored by phase contrast microscopy. After sufficient
655 myotube detachment was observed, Trypsin/EDTA solution was carefully aspirated
656 and a myotube-enriched suspension was collected by rinsing the plates five times with
657 normal growth medium. Enriched myotubes were then plated on glass coverslips
658 coated with 25 µg/ml fibronectin in PBS for >45 min at 37°C. After 24 h incubation at
659 37°C myotube cultures were subjected to siRNA treatment and/or microtubule
660 regrowth assays.

661

662 **MRF plasmids construction**

663 Primers used to generate fragments are listed in the table below. *Myod* and *Myog*
664 cDNA were obtained by reverse transcription PCR using RNA from C2C12 cells
665 differentiated for 2 days. The cDNAs were then cloned into the peGFP-N1 backbone
666 by Cold Fusion Cloning (System Biosciences, Cat# MC010B-1) following the
667 manufacturer's instruction. Positive clones were identified by restriction digest and
668 Sanger sequencing.

Oligonucleotides	Sequence
Primer: mouse MyoD cold fusion cloning forward	gggatccaccggtcgccaccatggagcttctatcgccgcc
Primer: mouse MyoD cold fusion cloning reverse	tcctcgcccttgctcaccataagcacctgataaatcgcat
Primer: mouse myogenin cold fusion cloning forward	gggatccaccggtcgccaccatggagctgtatgagacatc
Primer: mouse myogenin cold fusion cloning reverse	tcctcgcccttgctcaccatgttgggcatggtttcgtctg

669

670 **Luciferase plasmids construction**

671 Candidate regulatory elements associated with myogenin binding in *Syne1* and *Akap6*
672 genes were identified from ENCODE data accessed through the SCREEN web
673 interface (https://screen.wenglab.org/). Potential promoter regions were amplified from
674 genomic DNA obtained from NIH3T3 cells using the primers listed in the table below.
675 After amplification, promoter fragments were cloned in front of the *Renilla* luciferase
676 ORF (*hRluc*) into the psiCHECK-2 vector (Promega, Cat# C8021; GenBank Accession
677 Number AY535007) using NEBuilder HiFi DNA Assembly Master Mix (New England
678 Biolabs, Cat# E2621L) according to the manufacturer's instructions.

Oligonucleotides	Sequence
Primer: psiCHECK™-2 assembly cloning forward	gctagccaccatggcttc
Primer: psiCHECK™-2 assembly cloning reverse	gtcgagccatgtgagcaaaag
Primer: AKAP6α promoter fragment assembly cloning forward	ttttgctcacatggctcgacgcaaaccatgattattatctaagtc

Primer: AKAP6α promoter fragment assembly cloning forward	tggaagccatggtggctagcaggagatgccttgtttgac
Primer: AKAP6β promoter fragment assembly cloning forward	ttttgctcacatggctcgactacagagaattaatgcttagaaac
Primer: AKAP6β promoter fragment assembly cloning reverse	tggaagccatggtggctagcgcttgcagtgaactgtaatg
Primer: Syne1-giant promoter fragment assembly cloning forward	ttttgctcacatggctcgacactctgtctctttcaacccaaacatc atgaacc
Primer: Syne1-giant promoter fragment assembly cloning reverse	tggaagccatggtggctagcggctgtgccctccctccc
Primer: Syne1-α promoter fragment assembly cloning forward	ttttgctcacatggctcgacgtgtcagattctgactcattg
Primer: Syne1-α promoter fragment assembly cloning reverse	tggaagccatggtggctagctggtcatgcttctaaataaaac

679

680 **Plasmid transfections**

681 Plasmid transfection into NIH3T3 cells was carried out with 500 ng DNA per well of a
682 24-well plate using 1 µl Lipofectamine LTX (Thermo Fisher Scientific, Cat# 15338100)
683 according to the manufacturer's instructions. Transfection complexes were formed by
684 incubating DNA with Lipofectamine LTX in Opti-MEM for 20 min at room temperature.
685 For transfection of luciferase constructs in HEK293T cells, 250 ng luciferase vector
686 and 250 ng myogenin-eGFP or eGFP control plasmid were used per well of a 24-well
687 plate. Transfection complexes were assembled by incubating DNA with PEI MAX
688 (Polysciences, Cat# 24765-1) in a 1:3 ratio in Opti-MEM for 20 min at room
689 temperature.

690

691 **siRNA transfections**

692 Cells were transfected using 2 µl Lipofectamine RNAiMAX reagent (Thermo Fisher
693 Scientific, Cat# 13778150) and 40 nM final siRNA concentration per well of a 24-well
694 plate. Transfection complexes were formed by incubating siRNA with RNAiMAX in
695 Opti-MEM for 20 min at room temperature. C2C12 cells were transfected 24 h prior to

696 induction of differentiation (~50% confluence) and enriched C2C12 myotubes were
697 transfected 24 h after re-plating. NIH3T3 were transfected with siRNA 48 h after
698 plasmid transfection. The following siRNAs have been used in this study:
699

Oligonucleotides and sequences	Source	Catalogue number
siRNA targeting sequence: mouse Myogenin AAUAAAGACUGGUUGCUAUCAAAAA	Integrated DNA technologies	Cat# mm.Ri.Myog.13.1
siRNA targeting sequence: mouse Akap6 GGACUACAUCAAGAACGAATT	Thermo Fischer Scientific	Cat# 4390771 s108732
Negative control (si-ctrl) siRNA	Integrated DNA technologies	Cat# 51-01-14-04

700

701 **Luciferase assay**

702 Luciferase activity was measured in Centro XS^3 LB 960 96-well plate reader
703 luminometer (BertholdTech, #50-6860) using the Dual-Luciferase® Reporter Assay
704 System (Promega, #E1910) according to the manufacturer's instructions. In brief,
705 HEK293T cells were harvested 48h after transfection in passive lysis buffer and stored
706 at -80°C until measurement. Activities of firefly luciferase (*hluc+*, internal control) and
707 *Renilla* luciferase (promoter activation) were measured sequentially for each sample.
708 Values of *Renilla* luciferase activity were normalized to those of firefly luciferase for
709 each measurement.
710

711 **Production of lentiviral vectors**

712 The lentiviral packaging plasmid psPAX2 and the VSV-G envelope plasmid pMD2.G
713 were gifts from Didier Trono (psPAX2: Addgene plasmid #12260;
714 http://n2t.net/addgene:12260; RRID: Addgene_12260; pMD2.G: Addgene plasmid
715 #12259; http://n2t.net/addgene:12259; RRID: Addgene_12259). The transfer plasmids
716 pLenti CMVtight Blast DEST (w762-1) and pLenti CMV rtTA3 Hygro (w785-1) used for

717 creating tetracycline-inducible cell lines were gifts from Eric Campeau (w762-1:
718 Addgene plasmid #26434; http://n2t.net/addgene:26434; RRID: Addgene_26434;
719 w785-1: Addgene plasmid #26730; http://n2t.net/addgene:26730; RRID:
720 Addgene_26730). The coding sequences of human myogenin (gift from Matthew
721 Alexander & Louis Kunkel (Addgene plasmid #78341 ; http://n2t.net/addgene:78341;
722 RRID: Addgene_78341) and mScarlet (Bindels et al., 2017) (gift from Dorus Gadella
723 (Addgene plasmid #85042; http://n2t.net/addgene:85042; RRID: Addgene_85042)
724 were cloned into w762-1 by NEBuilder® HiFi DNA Assembly according to the
725 manufacturer's instructions using the primers indicated in the table below.

726 To produce lentiviral vectors, psPAX2, pMD2.G, and the desired transfer plasmid
727 were transfected in a 1:1:2 ratio into HEK293T cells using PEI MAX. Supernatant
728 containing lentiviral vectors was harvested 72h after transfection, filtered through a
729 0.45 µm filter and aliquots were snap frozen.

730

Oligonucleotides	Sequence
Primer: human myogenin cloning into pLenti CMVtight Blast DEST forward	agccgccaccATGGAGCTGTATGAGACATC
Primer: human myogenin cloning into pLenti CMVtight Blast DEST reverse	ctgccctctccactgcccatGTTGGGCATGGTTTCATC
Primer: mScarlet cloning into pLenti CMVtight Blast DEST forward	tcctggcccaATGGTGAGCAAGGGCGAG
Primer: mScarlet cloning into pLenti CMVtight Blast DEST reverse	ggccgccactgtgctggataTCACTTGTACAGCTCGTCCATGC

731

732 **Generation of stable cell lines**

733 Lentiviral vector aliquots were rapidly thawed at 37°C and diluted in tetracycline-free
734 growth medium containing 10 µg/ml Polybrene (Sigma-Aldrich, Cat# 107689). Cells
735 were transduced overnight in 6-well plates using 1 ml of diluted lentiviral vector. The
736 following morning, medium was refreshed and cells were selected for transgene

737 integration 72h after transduction. We first generated cells expressing a reverse
738 tetracycline activator (rtTA3), which were subsequently transduced with lentiviral
739 vectors carrying the desired transgene to express mScarlet or MYOG-2A-mScarlet
740 under control of a tetracycline responsive element (TRE). After selection, Tet-ON cell
741 lines were used for 20 passages.
742

743 **RT-PCR**

744 RNA was isolated using a column-based RNA purification kit. For production of cDNA,
745 1 µg of RNA was reverse transcribed using Oligo (dT) 12-18mer primers and M-MLV
746 Reverse Transcriptase (Sigma-Aldrich #M1302) according to the manufacturer's
747 instructions. For PCR, ~20 ng of cDNA were used with Redtaq master mix (Genaxxon
748 #M3029) and products were analyzed using agarose gel electrophoresis.

Primers	Sequence
mAkap6β forward	TCTAAAGCAGTTAGGCCCACAG
mAkap6β reverse	CTTCGGATGAGCTCGGGAAAT
nesprin-1α forward	GAAGGACTGAGCCTTTCGCTC
nesprin-1α reverse	GGGCTTGGCCAACTCTGAC
Gapdh forward	CAGAAGACTGTGGATGGCCC
Gapdh reverse	AGTGTAGCCCAGGATGCCCT

749

750 **Immunoprecipitation**

751 Cells were harvested in lysis buffer containing 1% NP-40, 150 mM NaCl, 10% glycerol,
752 5 mM EDTA, 20 mM Tris-HCl (pH 7) and EDTA-free protease inhibitor cocktail
753 (cOmplete™, Roche # 11873580001). After 30 min incubation on ice, samples were
754 sonicated and lysates were cleared by centrifugation at 16000xg for 16 min at 4°C. For
755 immunoprecipitation, 0.5 µg anti-AKAP6 antibody/mg of total protein were added to the
756 lysate and incubated overnight at 4°C on a rotor. Subsequently, antibody complexes

757 were purified by incubation of lysate with Protein A Sepharose® beads (Merck, GE17-
758 5138-01) for 3h rotating at 4°C. Beads were washed three times with cold lysis buffer
759 for 5 min and proteins were eluted from beads by incubation in 2x NuPAGE LDS
760 sample buffer () at 95°C for 5 min. Lysates and immunoprecipitated samples were
761 analyzed by SDS-PAGE (4-12% NuPAGE Novex Bis-Tris gels) under reducing
762 conditions and transferred to a nitrocellulose membrane by wet transfer at 350 mA and
763 <60 V for 1.5 h in 1x transfer buffer (25 mM Tris-HCl, pH 7.5, 192 mM glycine, 0.1%
764 SDS, 10% methanol). The membrane was then blocked with 5% BSA in TBS-T
765 (1×TBS, 0.05% Tween-20) and incubated with the following antibodies:

Antibodies and dilutions	Source	Catalogue number/ Identifier
rabbit polyclonal anti-PCM1 (H-262) dilution: 1:500	Santa Cruz	Cat# sc-67204, RRID:AB_2139591
rabbit polyclonal anti-Akap6 dilution: 1:2000	Sigma-Aldrich	Cat# HPA048741, RRID:AB_2680506
sheep polyclonal anti-rabbit IgG HRP-linked	GE Healthcare	NA934-1ML, RRID:AB_2722659

766

767 **ChIP-qPCR**

768 Protein and DNA were cross-linked by fixing cells for 10 min at 37°C using 1%
769 formaldehyde in culture medium. Cross-linking was quenched by adding 125 mM
770 glycine and gently agitating the cells for 5 min at room temperature. Then, cells were
771 harvested in ice-cold PBS, centrifuged at 1000xG for 5 min at 4°C, and the resulting
772 pellet was lysed in ChIP lysis buffer (1% SDS, 10 mM EDTA, 50 mM Tris-HCl pH 8.1)
773 for 30 min on ice. After lysis, samples were sonicated for 30 cycles consisting of 20s
774 sonication and 30s pause inside an ice bath. Sonicated samples were centrifuged at
775 4°C for 30 min at 10000xG. A small aliquot of the supernatant was saved as input
776 control and the remaining supernatant was subjected to immunoprecipitation. Samples
777 were diluted 1:5 in RIPA buffer and incubated overnight at 4°C with 1 µg/ml myogenin

778 antibody (Santa Cruz Biotechnology, #sc-12732 X) or IgG1 isotype control (Thermo
779 Fisher, # 16471482). Protein G agarose beads (Roche #11719416001) pre-blocked
780 with salmon sperm (Thermo Fisher, # 15632011) were used to precipitate antibody
781 complexes from diluted samples. Beads were sequentially washed at 4°C with low salt
782 buffer (0.1% SDS, 1% Triton X-100, 2 mM EDTA, 20 mM Tris-HCl pH 8.0, 150 mM
783 NaCl), high salt buffer (0.1% SDS, 1% Triton X-100, 2 mM EDTA, 20 mM Tris-HCl pH
784 8.0, 500 mM NaCl), LiCl buffer (0.25 M LiCl, 1% NP-40, 1% Sodium Deoxycholate,
785 1 mM EDTA, 10 mM Tris-HCl pH 8.0), and TE buffer (10 mM Tris-HCl pH 8.0, 1 mM
786 EDTA). Antibody complexes were eluted by incubating beads for 15 min at 30°C in
787 elution buffer (1% SDS, 100 mM $NaHCO_3$). Eluates were digested with proteinase K
788 and RNAse A and DNA fragments were purified using a PCR purification kit
789 (Macherey-Nagel, #740609).

ChIP-primers	Sequence
Akap6 β E box forward	GTTTCCTTGTGCAGCAGAGC
Akap6 β E box reverse	TGGTCTGTTGGTGTGGTGTT
Akap6 α E box forward	CCAGATTTTAACCCCAGAAG
Akap6 α E box reverse	AGTGCACAGACTAATAATCG
Syne1 α E box forward	TGCTCTTGGTGGACAAATGGT
Syne1 α E box reverse	TCTTTTGAGCCGTAACCTGCT
Syne1 giant E box forward	CGCTAGCGAACGCCTCTTC
Syne1 giant E box reverse	GGAGGGACAGATCCTTTAGGC
Syne 1 intron forward	TACATTTGCCTCGTGGCTGT
Syne 1 intron reverse	TGTGCTTTAGCCTGGAGTGG
Akap6 intron forward	CCTGTCCTTTCTGCGTCGAT
Akap6 intron reverse	GTAACCCGCCAGAGAAAACG
Desmin promoter forward	GTCTTCTGTCCTCTTGGGGCTGTCCA
Desmin promoter reverse	TGGAGTGGATGTGAAGATGGGTGAC

790

791 **Immunofluorescence and microscopy**

792 Antibodies used in this study are listed in the table below. Note that the MANNES1E
793 antibody detects different nesprin-1 isoforms (Holt et al., 2016; Randles et al., 2010).
794 However, previous studies have shown that only the nesprin-1α isoform is up-regulated
795 during muscle differentiation (Espigat-Georger et al., 2016; Gimpel et al., 2017; Holt et
796 al., 2016). Prior to fixation, cells were rinsed once with PBS. Cells were fixed either
797 with pre-chilled methanol at -20°C for 3 min or with 4% formaldehyde/PBS for 10 min
798 at room temperature. Formaldehyde-fixed cells were permeabilized with 0.5% TritonX-
799 100/PBS. Prior to antibody staining, samples were blocked for at least 20 min using
800 5% BSA in 0.2% Tween-20 in PBS. Primary antibodies were diluted in blocking reagent
801 and incubated with the sample for 90 min at room temperature or overnight at 4°C.
802 After removal of primary antibody solution and three 5 min washes with 0.1%
803 NP40/PBS, samples were incubated for 60 min with fluorophore-coupled secondary
804 antibodies. DNA was visualized with 0.5 µg/ml DAPI (4′,6′-diamidino-2-phenylindole)
805 in 0.1% NP40/PBS. After DAPI staining cover slips were rinsed once with Millipore-
806 filtered water and then mounted using Fluoromount-G mounting medium. Analysis,
807 image acquisition and high-resolution microscopy were done using a LSM800 confocal
808 laser scanning microscope equipped with an Airyscan detector and the ZEISS Blue
809 software (Carl Zeiss AG, RRID: SCR_013672) with Airyscan image processing.

Antibodies and dilutions	Source	Catalogue number/ Identifier
rabbit polyclonal anti-PCM1 (H-262) dilution: 1:200	Santa Cruz	Cat# sc-67204, RRID:AB_2139591
mouse monoclonal anti-PCM1 (G-6) dilution: 1:200	Santa Cruz	Cat# sc-398365
rabbit polyclonal anti-Akap6 dilution: 1:1000	Sigma-Aldrich	Cat# HPA048741, RRID:AB_2680506
mouse monoclonal anti-nesprin-1 (MANNES1E) dilution: 1:50	G. Morris (Randles et al., 2010)	N/A

mouse monoclonal anti-Myogenin (F5D) dilution 1:500	Santa Cruz	Cat# sc-12732, RRID:AB_627980
mouse monoclonal anti-MyoD1 dilution: 1:500	Millipore	Cat# MAB3878, RRID:AB_2251119
rat anti-α-tubulin dilution: 1:500	Sigma-Aldrich	Cat# T9026, RRID:AB_477593
goat polyclonal anti-Troponin I dilution: 1:500	Abcam	Cat# ab56357, RRID:AB_880622
mouse monoclonal anti-γ-tubulin dilution: 1:100	Santa Cruz	Cat# sc-51715, RRID:AB_630410
rabbit polyclonal anti-Akap9 dilution: 1:200	Sigma-Aldrich	Cat# HPA026109, RRID:AB_1844688
rabbit polyclonal anti-Pericentrin dilution: 1:1000	BioLegend	Cat# PRB-432C, RRID:AB_291635
Donkey anti-Rabbit IgG (H+L) Highly Cross-Adsorbed Secondary Antibody, Alexa Fluor 488 dilution: 1:500	Thermo Fisher Scientific	Cat# A21206
Donkey anti-Rabbit IgG (H+L) Highly Cross-Adsorbed Secondary Antibody, Alexa Fluor 594 dilution: 1:500	Thermo Fisher Scientific	Cat# A21207
Donkey anti-Rabbit IgG (H+L) Highly Cross-Adsorbed Secondary Antibody, Alexa Fluor 647 dilution: 1:500	Thermo Fisher Scientific	Cat# A31573
Donkey anti-Mouse IgG (H+L) Highly Cross-Adsorbed Secondary Antibody, Alexa Fluor 488 dilution: 1:500	Thermo Fisher Scientific	Cat# A21202
Donkey anti-Mouse IgG (H+L) Highly Cross-Adsorbed Secondary Antibody, Alexa Fluor 594 dilution: 1:500	Thermo Fisher Scientific	Cat# A21203
Donkey anti-Mouse IgG (H+L) Highly Cross-Adsorbed Secondary Antibody, Alexa Fluor 647 dilution: 1:500	Thermo Fisher Scientific	Cat# A31571

Donkey anti-Goat IgG (H+L) Highly Cross-Adsorbed Secondary Antibody, Alexa Fluor 647 dilution: 1:500	Thermo Fisher Scientific	Cat# A21447
Donkey anti-Rat IgG (H+L) Highly Cross-Adsorbed Secondary Antibody, Alexa Fluor 594 dilution: 1:500	Thermo Fisher Scientific	Cat# A21209

810

811 **Image analysis**

812 All image analyses were carried out using Fiji (http://fiji.sc, RRID: SCR_002285). For
813 quantification of nuclear envelope coverage, confocal images were transformed into
814 binary images by setting a manual intensity threshold. Regions of interests (ROI) were
815 obtained by detecting nuclei outline via DAPI staining and subsequent transformation
816 of these outlines into 1 µm-wide bands. Coverage was quantified as the percentage of
817 positive pixels inside bands in the binary images. ROIs for measuring intensities at
818 centrosomes were generated by detecting local signal maxima in γ-tubulin channels
819 and subsequent generation of circular ROIs with 1 µm diameter using the maxima as
820 centers.

821 To measure nuclear envelope intensity profiles for nesprin-1α and AKAP6, we first
822 created ROIs by manually detected nuclear outlines using DAPI staining. We then
823 decreased the diameter of these ROIs by 1 µm and used the newly created ROIS as
824 starting points for linear intensity profiles perpendicular to the nuclear outlines.

825

826 **Microtubule regrowth assay**

827 C2C12 cells were treated with 5 µM nocodazole (Sigma-Aldrich, Cat# M1404) in
828 culture media for 3 h at 37°C to depolymerize microtubules. To observe microtubule
829 regrowth, nocodazole-containing medium was removed, cells were rinsed three times
830 with cold medium and either fixed (0 min time point) with 4% formaldehyde in PBS for
831 10 min or immediately transferred to 37°C pre-warmed culture media for the desired

832 length of time followed by formaldehyde fixation. Myotubes were extracted with 1%
833 Triton X-100 in PHEM buffer (60 mM PIPES, 25 mM HEPES, 10 mM EGTA, 2 mM
834 MgCl2, pH 6.9) for 30 s at room temperature prior to fixation.
835
836 **Bioinformatics analysis**
837 Data was analyzed with R (http://www.r-project.org/; RRID:SCR_001905) and
838 Bioconductor (http://www.bioconductor.org/, RRID: SCR_006442). Myogenin ChIP-
839 Seq data (GEO accession number: GSE36024) produced within the ENCODE project
840 (Consortium, 2012; Consortium et al., 2020; Yue et al., 2014) were obtained via the
841 UCSC Genome Browser at https://genome.ucsc.edu/index.html (Kent et al., 2002;
842 Rosenbloom et al., 2013). NarrowPeak tracks relative to ChIP-Seq data from four
843 different time points were considered: undifferentiated C2C12 myoblasts as well as
844 C2C12 cultures differentiated for 24 h, 60 h, or 7 days. To identify myogenin promoter
845 binding, peaks were annotated to the Ensembl release 67 mouse genome relying on
846 Bioconductor packages biomaRt v. 2.30.0 (Durinck, Spellman, Birney, & Huber, 2009)
847 and ChIPpeakAnno v. 3.8.9 (Zhu et al., 2010). Genes were considered as myogenin
848 targets if a peak (p-value < 10^{-5}) was localized at a maximum distance of 1 kb from the
849 annotated transcriptional start site.
850 Results of differential expression analysis for RNA-Seq data from C2C12
851 differentiation (GEO accession number: GSE84158) were obtained from the Gene
852 Expression Omnibus (GEO) repository (Doynova et al., 2017). Three sample types
853 were analyzed: C2C12 myoblasts (C1), C2C12 cultures differentiated for 3 days
854 containing myoblasts as well as myotubes (C2), and C2C12 cultures differentiated for
855 7 days and treated with AraC resulting in depletion of proliferating myoblasts (C3).
856 Genes were considered as up-regulated if they exhibited a positive fold change
857 (p-value < 0.05) from C1 to C2 as well as from C1 to C3.

858 Gene expression microarray data for rat heart development were obtained as
859 described previously using the Affymetrix GeneChip RAT 230 Expression Set (Patra
860 et al., 2011). Genes were considered up-regulated if: 1) the corresponding probe set
861 was identified as differentially expressed on the basis of a procedure that accounts for
862 the total area under the profile compared to a constant profile (Di Camillo, Toffolo, Nair,
863 Greenlund, & Cobelli, 2007), and 2) the difference between the maximum expression
864 value over time and the initial one was greater than the difference between the initial
865 value and the minimum value.

866 For Gene Ontology analysis, annotated cellular component terms for each of the
867 potential myogenin targets were retrieved using the search tool at
868 http://geneontology.org/ (Ashburner et al., 2000; The Gene Ontology, 2017). Potential
869 targets annotated with the terms “nuclear membrane” and “nuclear envelope” were
870 considered.

871

872 **QUANTIFICATION AND STATISTICAL ANALYSIS**

873 **Quantification of nesprin-1α$^+$ nuclei**

874 Low levels of nesprin-1 expression can be detected at nuclei of non-differentiated
875 muscle cells using MANNES1E antibody. Prior to scoring of nesprin-1α$^+$ nuclei, we
876 therefore set a threshold for nesprin-1 signal in images of differentiated C2C12 cells
877 by measuring and subtracting maximal nesprin-1 signal intensity in undifferentiated
878 C2C12 cultures.

879

880 **Statistical analysis**

881 As preliminary experiments indicated a large effect size of siRNA treatments and
882 ectopic MRF expression, three biological replicates were performed per experiment
883 (i.e. n = 3). Biological replicate means that cells were freshly plated, treated, fixed and

884 stained, and then analyzed. For each biological replicate, two technical replicates were
885 performed in the sense that two individual wells were processed at the same time.
886 When analyzed, the two technical replicates were scored as one sample.

887 For quantification in C2C12 cells, >500 nuclei were analyzed per condition and
888 biological replicate. For MRF-GFP experiments, >50 GFP^+ cells were analyzed per
889 condition and biological replicate. For nuclear coverage and intensity quantifications of
890 mScarlet and MYOG-mScarlet cells, >100 nuclei or centrosomes were analyzed per
891 condition and pooled from three biological replicates to display distribution in violin
892 plots.

893 Statistical analysis was carried out using GraphPad Prism 5.02 or Prism 8.2.1
894 (La Jolla, USA). Differences between groups were considered statistically significant
895 when the p-value ≤ 0.05. The 95% confidence interval (CI) for the differences between
896 compared groups are reported in the figure legends. Statistical significance of
897 differences between groups was tested using the following:

898

899 **Figures 1F, 1H, 1S1B-C, 2S2A-C, 4S1A-B, 5B, 5S3A-B, 7E:** One-way ANOVA
900 followed by Bonferroni's Post-Hoc test to compare selected pairs of groups.

901 **Figures 2B, 6C, 7B, 7D, 7F:** Student's t-test together with an F-test to assess equality
902 of variances.

903 **Figures 2D, 2F, 2H, 2M, 3B, 3D-E, 5D-F, 5S2A-B:** Kolmogorov-Smirnov test to
904 compare the cumulative distribution of groups.

905

906 **Acknowledgments**

907 We acknowledge the Platform for Immortalization of Human Cells at the Institute de
908 Myologie, Paris for the generation and distribution of immortalized human myoblasts.
909 We thank Glenn E. Morris for providing us with nesprin-1 antibody (MANNES1E). We
910 thank the ENCODE consortium, the laboratory of Barbara Wold and the Millard and
911 Muriel Jacobs Genetics and Genomics Laboratory at the California Institute of
912 Technology for providing myogenin ChIP-Seq data. We thank Christina Warnecke for
913 support with ChIP experiments, Marc Stemmler, Eva Bauer, and Thomas Brabletz for
914 their help with luciferase assays and Anna K. Großkopf and Alexander S. Hahn for
915 experimental support. We acknowledge Les Laboratoires Servier for providing
916 illustrations in the Servier Medical Art collection under a Creative Commons Attribution
917 3.0 Unported License (https://creativecommons.org/ licenses/by/3.0/). We thank Anna
918 K. Großkopf, Manfred Frasch, Hanh Nguyen, Thomas U. Mayer, Rosa M. Puertollano,
919 Payel Das, Marina Leone, Gentian Musa, and Salvador Cazorla-Vazquez for critical
920 reading of the manuscript and all members of the Engel lab for critical discussions.

921 This work was supported by the Interdisciplinary Centre for Clinical Research
922 Erlangen (IZKF project J42 to F.F.), the Emerging Fields Initiative Cell "Cycle in
923 Disease and Regeneration" (CYDER to F.B.E.) and an ELAN Program Grant (ELAN-
924 16-01-04-1-Vergarajauregui to S.V.) from the Friedrich-Alexander-Universität
925 Erlangen-Nürnberg, by the German Research Foundation (DFG, INST 410/91-1
926 FUGG and EN 453/12-1 to F.B.E.), and by the Research Foundation Medicine at the
927 University Clinic Erlangen, Germany.

928

929 **Declaration of Interests**

930 The authors have no conflict of interest to declare.

931

932 ## Figures

933 Figure 1. Myogenin is required for MTOC protein localization to the nuclear envelope.
934 Figure 2. Myogenin expression is sufficient to induce NE-MTOC formation in non-muscle cells.
935 Figure 3. Myogenin expression attenuates the centrosomal MTOC.
936 Figure 4. The nesprin-1α interaction partner AKAP6 is a potential mediator of myogenin-induced NE-
937 MTOC formation.
938 Figure 5. AKAP6 is required for the nuclear envelope localization of MTOC proteins.
939 Figure 6. AKAP6 is required for correct nuclear positioning in myotubes.
940 Figure 7. Myogenin preferentially induces MTOC-associated isoforms of *Syne1* and *Akap6.*
941 Figure 8. Schematic overview of the role of myogenin and AKAP6 in NE-MTOC formation.
942
943
944 ## Figure supplements

945 Figure 1 – figure supplement 1. Intermediate stages of MTOC protein localization to the nuclear
946 envelope.
947 Figure 1 – figure supplement 2. PCM-1 exhibits a centrosomal localization pattern at nesprin-1^{+} nuclei
948 in myogenin-depleted C2C12 cells.
949 Figure 2 – figure supplement 1. Myogenin is required for MyoD-induced nuclear envelope recruitment
950 of PCM-1.
951 Figure 2 – figure supplement 2. Myogenin targets are specifically precipitated in induced MYOG-
952 mScarlet cells.
953 Figure 2 – figure supplement 3. Microtubule depolymerization in mScarlet and MYOG-mScarlet cells.
954 Figure 4 – figure supplement 1. The myogenin antibody specifically precipitates the Akap6β promoter
955 region in induced MYOG-mScarlet cells.
956 Figure 4 – figure supplement 2. Quantification of nesprin-1α and AKAP6 signal at the nuclear envelope.
957 Figure 5 – figure supplement 1. AKAP6 depletion does not affect nesprin-1α.
958 Figure 5 – figure supplement 2. AKAP6 or nesprin-1α depletion does not prevent centrosome attenuation
959 in MYOG-expressing cells.
960 Figure 5 – figure supplement 3. MyoD induces nesprin-1α and AKAP6.
961 Figure 6 – figure supplement 1. AKAP6 depletion does not affect steady state microtubule organization
962 but reduces detyrosinated microtubules.
963 Figure 7 – figure supplement 1. Ectopic co-expression of nesprin-1α and AKAP6β is not sufficient for
964 MTOC function at the nuclear envelope.
965

References

Akhmanova, A., & Steinmetz, M. O. (2015). Control of microtubule organization and dynamics: two ends in the limelight. *Nat Rev Mol Cell Biol, 16*(12), 711-726. doi:10.1038/nrm4084

Apel, E. D., Lewis, R. M., Grady, R. M., & Sanes, J. R. (2000). Syne-1, a dystrophin- and Klarsicht-related protein associated with synaptic nuclei at the neuromuscular junction. *J Biol Chem, 275*(41), 31986-31995. doi:10.1074/jbc.M004775200

Arnandis, T., Monteiro, P., Adams, S. D., Bridgeman, V. L., Rajeeve, V., Gadaleta, E., . . . Godinho, S. A. (2018). Oxidative Stress in Cells with Extra Centrosomes Drives Non-Cell-Autonomous Invasion. *Dev Cell, 47*(4), 409-424 e409. doi:10.1016/j.devcel.2018.10.026

Ashburner, M., Ball, C. A., Blake, J. A., Botstein, D., Butler, H., Cherry, J. M., . . . Sherlock, G. (2000). Gene ontology: tool for the unification of biology. The Gene Ontology Consortium. *Nat Genet, 25*(1), 25-29. doi:10.1038/75556

Becker, R., Leone, M., & Engel, F. B. (2020). Microtubule Organization in Striated Muscle Cells. *Cells, 9*(6). doi:10.3390/cells9061395

Berkes, C. A., & Tapscott, S. J. (2005). MyoD and the transcriptional control of myogenesis. *Semin Cell Dev Biol, 16*(4-5), 585-595. doi:10.1016/j.semcdb.2005.07.006

Bindels, D. S., Haarbosch, L., van Weeren, L., Postma, M., Wiese, K. E., Mastop, M., . . . Gadella, T. W., Jr. (2017). mScarlet: a bright monomeric red fluorescent protein for cellular imaging. *Nat Methods, 14*(1), 53-56. doi:10.1038/nmeth.4074

Braun, T., Bober, E., Winter, B., Rosenthal, N., & Arnold, H. H. (1990). Myf-6, a new member of the human gene family of myogenic determination factors: evidence for a gene cluster on chromosome 12. *EMBO J, 9*(3), 821-831. Retrieved from https://www.ncbi.nlm.nih.gov/pubmed/2311584

Braun, T., Buschhausen-Denker, G., Bober, E., Tannich, E., & Arnold, H. H. (1989). A novel human muscle factor related to but distinct from MyoD1 induces myogenic conversion in 10T1/2 fibroblasts. *EMBO J, 8*(3), 701-709. Retrieved from https://www.ncbi.nlm.nih.gov/pubmed/2721498

Braun, T., & Gautel, M. (2011). Transcriptional mechanisms regulating skeletal muscle differentiation, growth and homeostasis. *Nat Rev Mol Cell Biol, 12*(6), 349-361. doi:10.1038/nrm3118

Brodu, V., Baffet, A. D., Le Droguen, P. M., Casanova, J., & Guichet, A. (2010). A developmentally regulated two-step process generates a noncentrosomal microtubule network in Drosophila tracheal cells. *Dev Cell, 18*(5), 790-801. doi:10.1016/j.devcel.2010.03.015

Buckingham, M., & Rigby, P. W. (2014). Gene regulatory networks and transcriptional mechanisms that control myogenesis. *Dev Cell, 28*(3), 225-238. doi:10.1016/j.devcel.2013.12.020

Bugnard, E., Zaal, K. J., & Ralston, E. (2005). Reorganization of microtubule nucleation during muscle differentiation. *Cell Motil Cytoskeleton, 60*(1), 1-13. doi:10.1002/cm.20042

1006 Chang, Y., Cho, B., Kim, S., & Kim, J. (2019). Direct conversion of fibroblasts to osteoblasts
1007 as a novel strategy for bone regeneration in elderly individuals. *Exp Mol Med, 51*(5), 1-
1008 8. doi:10.1038/s12276-019-0251-1

1009 Chen, C. Y., Caporizzo, M. A., Bedi, K., Vite, A., Bogush, A. I., Robison, P., . . . Prosser, B. L.
1010 (2018). Suppression of detyrosinated microtubules improves cardiomyocyte function in
1011 human heart failure. *Nat Med, 24*(8), 1225-1233. doi:10.1038/s41591-018-0046-2

1012 Chen, J. V., Buchwalter, R. A., Kao, L. R., & Megraw, T. L. (2017). A Splice Variant of
1013 Centrosomin Converts Mitochondria to Microtubule-Organizing Centers. *Curr Biol,*
1014 *27*(13), 1928-1940 e1926. doi:10.1016/j.cub.2017.05.090

1015 Comai, G., & Tajbakhsh, S. (2014). Molecular and cellular regulation of skeletal myogenesis.
1016 *Curr Top Dev Biol, 110*, 1-73. doi:10.1016/B978-0-12-405943-6.00001-4

1017 Conduit, P. T., Wainman, A., & Raff, J. W. (2015). Centrosome function and assembly in animal
1018 cells. *Nat Rev Mol Cell Biol, 16*(10), 611-624. doi:10.1038/nrm4062

1019 Consortium, E. P. (2012). An integrated encyclopedia of DNA elements in the human genome.
1020 *Nature, 489*(7414), 57-74. doi:10.1038/nature11247

1021 Consortium, E. P., Moore, J. E., Purcaro, M. J., Pratt, H. E., Epstein, C. B., Shoresh, N., . . .
1022 Weng, Z. (2020). Expanded encyclopaedias of DNA elements in the human and mouse
1023 genomes. *Nature, 583*(7818), 699-710. doi:10.1038/s41586-020-2493-4

1024 Dammermann, A., & Merdes, A. (2002). Assembly of centrosomal proteins and microtubule
1025 organization depends on PCM-1. *J Cell Biol, 159*(2), 255-266.
1026 doi:10.1083/jcb.200204023

1027 Davis, R. L., Weintraub, H., & Lassar, A. B. (1987). Expression of a single transfected cDNA
1028 converts fibroblasts to myoblasts. *Cell, 51*(6), 987-1000. doi:10.1016/0092-
1029 8674(87)90585-x

1030 Di Camillo, B., Toffolo, G., Nair, S. K., Greenlund, L. J., & Cobelli, C. (2007). Significance
1031 analysis of microarray transcript levels in time series experiments. *BMC Bioinformatics,*
1032 *8 Suppl 1*, S10. doi:10.1186/1471-2105-8-S1-S10

1033 Doynova, M. D., Markworth, J. F., Cameron-Smith, D., Vickers, M. H., & O'Sullivan, J. M.
1034 (2017). Linkages between changes in the 3D organization of the genome and
1035 transcription during myotube differentiation in vitro. *Skelet Muscle, 7*(1), 5.
1036 doi:10.1186/s13395-017-0122-1

1037 Durinck, S., Spellman, P. T., Birney, E., & Huber, W. (2009). Mapping identifiers for the
1038 integration of genomic datasets with the R/Bioconductor package biomaRt. *Nat Protoc,*
1039 *4*(8), 1184-1191. doi:10.1038/nprot.2009.97

1040 Edmondson, D. G., & Olson, E. N. (1989). A gene with homology to the myc similarity region
1041 of MyoD1 is expressed during myogenesis and is sufficient to activate the muscle
1042 differentiation program. *Genes Dev, 3*(5), 628-640. doi:10.1101/gad.3.5.628

1043 Elhanany-Tamir, H., Yu, Y. V., Shnayder, M., Jain, A., Welte, M., & Volk, T. (2012). Organelle
1044 positioning in muscles requires cooperation between two KASH proteins and
1045 microtubules. *J Cell Biol, 198*(5), 833-846. doi:10.1083/jcb.201204102

1046 Espigat-Georger, A., Dyachuk, V., Chemin, C., Emorine, L., & Merdes, A. (2016). Nuclear
1047 alignment in myotubes requires centrosome proteins recruited by nesprin-1. *J Cell Sci,*
1048 *129*(22), 4227-4237. doi:10.1242/jcs.191767

1049 Gimpel, P., Lee, Y. L., Sobota, R. M., Calvi, A., Koullourou, V., Patel, R., . . . Gomes, E. R.
1050 (2017). Nesprin-1alpha-Dependent Microtubule Nucleation from the Nuclear Envelope
1051 via Akap450 Is Necessary for Nuclear Positioning in Muscle Cells. *Curr Biol, 27*(19),
1052 2999-3009 e2999. doi:10.1016/j.cub.2017.08.031

1053 Godinho, S. A., & Pellman, D. (2014). Causes and consequences of centrosome abnormalities
1054 in cancer. *Philos Trans R Soc Lond B Biol Sci, 369*(1650). doi:10.1098/rstb.2013.0467

1055 Godinho, S. A., Picone, R., Burute, M., Dagher, R., Su, Y., Leung, C. T., . . . Pellman, D. (2014).
1056 Oncogene-like induction of cellular invasion from centrosome amplification. *Nature,*
1057 *510*(7503), 167-171. doi:10.1038/nature13277

1058 Hasty, P., Bradley, A., Morris, J. H., Edmondson, D. G., Venuti, J. M., Olson, E. N., & Klein,
1059 W. H. (1993). Muscle deficiency and neonatal death in mice with a targeted mutation
1060 in the myogenin gene. *Nature, 364*(6437), 501-506. doi:10.1038/364501a0

1061 Heffler, J., Shah, P. P., Robison, P., Phyo, S., Veliz, K., Uchida, K., . . . Prosser, B. L. (2020).
1062 A Balance Between Intermediate Filaments and Microtubules Maintains Nuclear
1063 Architecture in the Cardiomyocyte. *Circ Res, 126*(3), e10-e26.
1064 doi:10.1161/CIRCRESAHA.119.315582

1065 Hinchcliffe, E. H., Miller, F. J., Cham, M., Khodjakov, A., & Sluder, G. (2001). Requirement of
1066 a centrosomal activity for cell cycle progression through G1 into S phase. *Science,*
1067 *291*(5508), 1547-1550. doi:10.1126/science.1056866

1068 Holt, I., Duong, N. T., Zhang, Q., Lam le, T., Sewry, C. A., Mamchaoui, K., . . . Morris, G. E.
1069 (2016). Specific localization of nesprin-1-alpha2, the short isoform of nesprin-1 with a
1070 KASH domain, in developing, fetal and regenerating muscle, using a new monoclonal
1071 antibody. *BMC Cell Biol, 17*(1), 26. doi:10.1186/s12860-016-0105-9

1072 Ieda, M., Fu, J. D., Delgado-Olguin, P., Vedantham, V., Hayashi, Y., Bruneau, B. G., &
1073 Srivastava, D. (2010). Direct reprogramming of fibroblasts into functional
1074 cardiomyocytes by defined factors. *Cell, 142*(3), 375-386.
1075 doi:10.1016/j.cell.2010.07.002

1076 Ishibashi, J., Perry, R. L., Asakura, A., & Rudnicki, M. A. (2005). MyoD induces myogenic
1077 differentiation through cooperation of its NH2- and COOH-terminal regions. *J Cell Biol,*
1078 *171*(3), 471-482. doi:10.1083/jcb.200502101

1079 Kapiloff, M. S., Schillace, R. V., Westphal, A. M., & Scott, J. D. (1999). mAKAP: an A-kinase
1080 anchoring protein targeted to the nuclear membrane of differentiated myocytes. *J Cell*
1081 *Sci, 112 (Pt 16)*, 2725-2736. Retrieved from
1082 http://www.ncbi.nlm.nih.gov/pubmed/10413680

1083 Kent, W. J., Sugnet, C. W., Furey, T. S., Roskin, K. M., Pringle, T. H., Zahler, A. M., & Haussler,
1084 D. (2002). The human genome browser at UCSC. *Genome Res, 12*(6), 996-1006.
1085 doi:10.1101/gr.229102

1086 Khodjakov, A., & Rieder, C. L. (2001). Centrosomes enhance the fidelity of cytokinesis in
1087 vertebrates and are required for cell cycle progression. *J Cell Biol, 153*(1), 237-242.
1088 Retrieved from http://www.ncbi.nlm.nih.gov/pubmed/11285289

1089 Klose, K., Gossen, M., & Stamm, C. (2019). Turning fibroblasts into cardiomyocytes:
1090 technological review of cardiac transdifferentiation strategies. *FASEB J, 33*(1), 49-70.
1091 doi:10.1096/fj.201800712R

1092 Kronebusch, P. J., & Singer, S. J. (1987). The microtubule-organizing complex and the Golgi
1093 apparatus are co-localized around the entire nuclear envelope of interphase cardiac
1094 myocytes. *J Cell Sci, 88 (Pt 1)*, 25-34. Retrieved from
1095 http://www.ncbi.nlm.nih.gov/pubmed/3327863

1096 Leask, A., Obrietan, K., & Stearns, T. (1997). Synaptically coupled central nervous system
1097 neurons lack centrosomal gamma-tubulin. *Neurosci Lett, 229*(1), 17-20.
1098 doi:10.1016/s0304-3940(97)00412-6

1099 Lechler, T., & Fuchs, E. (2007). Desmoplakin: an unexpected regulator of microtubule
1100 organization in the epidermis. *J Cell Biol, 176*(2), 147-154. doi:10.1083/jcb.200609109

1101 Lee, C., Scherr, H. M., & Wallingford, J. B. (2007). Shroom family proteins regulate gamma-
1102 tubulin distribution and microtubule architecture during epithelial cell shape change.
1103 *Development, 134*(7), 1431-1441. doi:10.1242/dev.02828

1104 Lee, S. W., Won, J. Y., Yang, J., Lee, J., Kim, S. Y., Lee, E. J., & Kim, H. S. (2015). AKAP6
1105 inhibition impairs myoblast differentiation and muscle regeneration: Positive loop
1106 between AKAP6 and myogenin. *Sci Rep, 5*, 16523. doi:10.1038/srep16523

1107 Levine, M. S., Bakker, B., Boeckx, B., Moyett, J., Lu, J., Vitre, B., . . . Holland, A. J. (2017).
1108 Centrosome Amplification Is Sufficient to Promote Spontaneous Tumorigenesis in
1109 Mammals. *Dev Cell, 40*(3), 313-322 e315. doi:10.1016/j.devcel.2016.12.022

1110 LoMastro, G. M., & Holland, A. J. (2019). The Emerging Link between Centrosome Aberrations
1111 and Metastasis. *Dev Cell, 49*(3), 325-331. doi:10.1016/j.devcel.2019.04.002

1112 Londhe, P., & Davie, J. K. (2011). Sequential association of myogenic regulatory factors and
1113 E proteins at muscle-specific genes. *Skelet Muscle, 1*(1), 14. doi:10.1186/2044-5040-
1114 1-14

1115 Luders, J. (2020). Nucleating microtubules in neurons: Challenges and solutions. *Dev*
1116 *Neurobiol*. doi:10.1002/dneu.22751

1117 Mamchaoui, K., Trollet, C., Bigot, A., Negroni, E., Chaouch, S., Wolff, A., . . . Mouly, V. (2011).
1118 Immortalized pathological human myoblasts: towards a universal tool for the study of
1119 neuromuscular disorders. *Skelet Muscle, 1*, 34. doi:10.1186/2044-5040-1-34

1120 Meads, T., & Schroer, T. A. (1995). Polarity and nucleation of microtubules in polarized
1121 epithelial cells. *Cell Motil Cytoskeleton, 32*(4), 273-288. doi:10.1002/cm.970320404

1122 Meng, W., Mushika, Y., Ichii, T., & Takeichi, M. (2008). Anchorage of microtubule minus ends
1123 to adherens junctions regulates epithelial cell-cell contacts. *Cell, 135*(5), 948-959.
1124 doi:10.1016/j.cell.2008.09.040

1125 Michel, J. J., Townley, I. K., Dodge-Kafka, K. L., Zhang, F., Kapiloff, M. S., & Scott, J. D. (2005).
1126 Spatial restriction of PDK1 activation cascades by anchoring to mAKAPalpha. *Mol Cell,*
1127 *20*(5), 661-672. doi:10.1016/j.molcel.2005.10.013

1128 Mulari, M. T., Patrikainen, L., Kaisto, T., Metsikko, K., Salo, J. J., & Vaananen, H. K. (2003).
1129 The architecture of microtubular network and Golgi orientation in osteoclasts--major

1130 differences between avian and mammalian species. *Exp Cell Res, 285*(2), 221-235.
1131 doi:10.1016/s0014-4827(03)00033-8

1132 Muroyama, A., Seldin, L., & Lechler, T. (2016). Divergent regulation of functionally distinct
1133 gamma-tubulin complexes during differentiation. *J Cell Biol, 213*(6), 679-692.
1134 doi:10.1083/jcb.201601099

1135 Nabeshima, Y., Hanaoka, K., Hayasaka, M., Esumi, E., Li, S., Nonaka, I., & Nabeshima, Y.
1136 (1993). Myogenin gene disruption results in perinatal lethality because of severe
1137 muscle defect. *Nature, 364*(6437), 532-535. doi:10.1038/364532a0

1138 Nguyen, M. M., McCracken, C. J., Milner, E. S., Goetschius, D. J., Weiner, A. T., Long, M. K.,
1139 . . . Rolls, M. M. (2014). Gamma-tubulin controls neuronal microtubule polarity
1140 independently of Golgi outposts. *Mol Biol Cell, 25*(13), 2039-2050.
1141 doi:10.1091/mbc.E13-09-0515

1142 Nguyen, M. M., Stone, M. C., & Rolls, M. M. (2011). Microtubules are organized independently
1143 of the centrosome in Drosophila neurons. *Neural Dev, 6*, 38. doi:10.1186/1749-8104-
1144 6-38

1145 Ori-McKenney, K. M., Jan, L. Y., & Jan, Y. N. (2012). Golgi outposts shape dendrite
1146 morphology by functioning as sites of acentrosomal microtubule nucleation in neurons.
1147 *Neuron, 76*(5), 921-930. doi:10.1016/j.neuron.2012.10.008

1148 Pare, G. C., Easlick, J. L., Mislow, J. M., McNally, E. M., & Kapiloff, M. S. (2005). Nesprin-
1149 1alpha contributes to the targeting of mAKAP to the cardiac myocyte nuclear envelope.
1150 *Exp Cell Res, 303*(2), 388-399. doi:10.1016/j.yexcr.2004.10.009

1151 Passariello, C. L., Li, J., Dodge-Kafka, K., & Kapiloff, M. S. (2015). mAKAP-a master scaffold
1152 for cardiac remodeling. *J Cardiovasc Pharmacol, 65*(3), 218-225.
1153 doi:10.1097/FJC.0000000000000206

1154 Patra, C., Diehl, F., Ferrazzi, F., van Amerongen, M. J., Novoyatleva, T., Schaefer, L., . . .
1155 Engel, F. B. (2011). Nephronectin regulates atrioventricular canal differentiation via
1156 Bmp4-Has2 signaling in zebrafish. *Development, 138*(20), 4499-4509.
1157 doi:10.1242/dev.067454

1158 Prosser, S. L., & Pelletier, L. (2015). Centrosome biology: the ins and outs of centrosome
1159 assembly. *Curr Biol, 25*(15), R656-659. doi:10.1016/j.cub.2015.06.038

1160 Prosser, S. L., & Pelletier, L. (2020). Centriolar satellite biogenesis and function in vertebrate
1161 cells. *J Cell Sci, 133*(1). doi:10.1242/jcs.239566

1162 Randles, K. N., Lam le, T., Sewry, C. A., Puckelwartz, M., Furling, D., Wehnert, M., . . . Morris,
1163 G. E. (2010). Nesprins, but not sun proteins, switch isoforms at the nuclear envelope
1164 during muscle development. *Dev Dyn, 239*(3), 998-1009. doi:10.1002/dvdy.22229

1165 Rosenbloom, K. R., Sloan, C. A., Malladi, V. S., Dreszer, T. R., Learned, K., Kirkup, V. M., . .
1166 . Kent, W. J. (2013). ENCODE data in the UCSC Genome Browser: year 5 update.
1167 *Nucleic Acids Res, 41*(Database issue), D56-63. doi:10.1093/nar/gks1172

1168 Ruehr, M. L., Russell, M. A., Ferguson, D. G., Bhat, M., Ma, J., Damron, D. S., . . . Bond, M.
1169 (2003). Targeting of protein kinase A by muscle A kinase-anchoring protein (mAKAP)
1170 regulates phosphorylation and function of the skeletal muscle ryanodine receptor. *J*
1171 *Biol Chem, 278*(27), 24831-24836. doi:10.1074/jbc.M213279200

Sanchez-Huertas, C., Freixo, F., Viais, R., Lacasa, C., Soriano, E., & Luders, J. (2016). Non-centrosomal nucleation mediated by augmin organizes microtubules in post-mitotic neurons and controls axonal microtubule polarity. *Nat Commun, 7*, 12187. doi:10.1038/ncomms12187

Sanchez, A. D., & Feldman, J. L. (2017). Microtubule-organizing centers: from the centrosome to non-centrosomal sites. *Curr Opin Cell Biol, 44*, 93-101. doi:10.1016/j.ceb.2016.09.003

Sir, J. H., Putz, M., Daly, O., Morrison, C. G., Dunning, M., Kilmartin, J. V., & Gergely, F. (2013). Loss of centrioles causes chromosomal instability in vertebrate somatic cells. *J Cell Biol, 203*(5), 747-756. doi:10.1083/jcb.201309038

Srsen, V., Fant, X., Heald, R., Rabouille, C., & Merdes, A. (2009). Centrosome proteins form an insoluble perinuclear matrix during muscle cell differentiation. *BMC Cell Biol, 10*, 28. doi:10.1186/1471-2121-10-28

Tassin, A. M., Maro, B., & Bornens, M. (1985). Fate of microtubule-organizing centers during myogenesis in vitro. *J Cell Biol, 100*(1), 35-46. Retrieved from http://www.ncbi.nlm.nih.gov/pubmed/3880758

Teixido-Travesa, N., Roig, J., & Luders, J. (2012). The where, when and how of microtubule nucleation - one ring to rule them all. *J Cell Sci, 125*(Pt 19), 4445-4456. doi:10.1242/jcs.106971

The Gene Ontology, C. (2017). Expansion of the Gene Ontology knowledgebase and resources. *Nucleic Acids Res, 45*(D1), D331-D338. doi:10.1093/nar/gkw1108

Toya, M., Kobayashi, S., Kawasaki, M., Shioi, G., Kaneko, M., Ishiuchi, T., . . . Takeichi, M. (2016). CAMSAP3 orients the apical-to-basal polarity of microtubule arrays in epithelial cells. *Proc Natl Acad Sci U S A, 113*(2), 332-337. doi:10.1073/pnas.1520638113

Venuti, J. M., Morris, J. H., Vivian, J. L., Olson, E. N., & Klein, W. H. (1995). Myogenin is required for late but not early aspects of myogenesis during mouse development. *J Cell Biol, 128*(4), 563-576. Retrieved from http://www.ncbi.nlm.nih.gov/pubmed/7532173

Vergarajauregui, S., Becker, R., Steffen, U., Sharkova, M., Esser, T., Petzold, J., . . . Engel, F. B. (2020). AKAP6 orchestrates the nuclear envelope microtubule-organizing center by linking golgi and nucleus via AKAP9. *Elife, 9*. doi:10.7554/eLife.61669

Wang, S., Reuveny, A., & Volk, T. (2015). Nesprin provides elastic properties to muscle nuclei by cooperating with spectraplakin and EB1. *J Cell Biol, 209*(4), 529-538. doi:10.1083/jcb.201408098

Weintraub, H., Tapscott, S. J., Davis, R. L., Thayer, M. J., Adam, M. A., Lassar, A. B., & Miller, A. D. (1989). Activation of muscle-specific genes in pigment, nerve, fat, liver, and fibroblast cell lines by forced expression of MyoD. *Proc Natl Acad Sci U S A, 86*(14), 5434-5438. doi:10.1073/pnas.86.14.5434

Yamamoto, K., Kishida, T., Sato, Y., Nishioka, K., Ejima, A., Fujiwara, H., . . . Mazda, O. (2015). Direct conversion of human fibroblasts into functional osteoblasts by defined factors. *Proc Natl Acad Sci U S A, 112*(19), 6152-6157. doi:10.1073/pnas.1420713112

Yang, R., & Feldman, J. L. (2015). SPD-2/CEP192 and CDK Are Limiting for Microtubule-Organizing Center Function at the Centrosome. *Curr Biol, 25*(14), 1924-1931. doi:10.1016/j.cub.2015.06.001

1215 Yue, F., Cheng, Y., Breschi, A., Vierstra, J., Wu, W., Ryba, T., . . . Mouse, E. C. (2014). A
1216 comparative encyclopedia of DNA elements in the mouse genome. *Nature, 515*(7527),
1217 355-364. doi:10.1038/nature13992

1218 Zebrowski, D. C., Vergarajauregui, S., Wu, C. C., Piatkowski, T., Becker, R., Leone, M., . . .
1219 Engel, F. B. (2015). Developmental alterations in centrosome integrity contribute to the
1220 post-mitotic state of mammalian cardiomyocytes. *Elife, 4*. doi:10.7554/eLife.05563

1221 Zhang, Q., Skepper, J. N., Yang, F., Davies, J. D., Hegyi, L., Roberts, R. G., . . . Shanahan,
1222 C. M. (2001). Nesprins: a novel family of spectrin-repeat-containing proteins that
1223 localize to the nuclear membrane in multiple tissues. *J Cell Sci, 114*(Pt 24), 4485-4498.
1224 Retrieved from http://www.ncbi.nlm.nih.gov/pubmed/11792814

1225 Zhang, X., Chen, M. H., Wu, X., Kodani, A., Fan, J., Doan, R., . . . Walsh, C. A. (2016). Cell-
1226 Type-Specific Alternative Splicing Governs Cell Fate in the Developing Cerebral
1227 Cortex. *Cell, 166*(5), 1147-1162 e1115. doi:10.1016/j.cell.2016.07.025

1228 Zhu, L. J., Gazin, C., Lawson, N. D., Pages, H., Lin, S. M., Lapointe, D. S., & Green, M. R.
1229 (2010). ChIPpeakAnno: a Bioconductor package to annotate ChIP-seq and ChIP-chip
1230 data. *BMC Bioinformatics, 11*, 237. doi:10.1186/1471-2105-11-237

1231

1232

Becker R *et al.*, Figure 1

Myogenin is required for MTOC protein localization to the nuclear envelope.

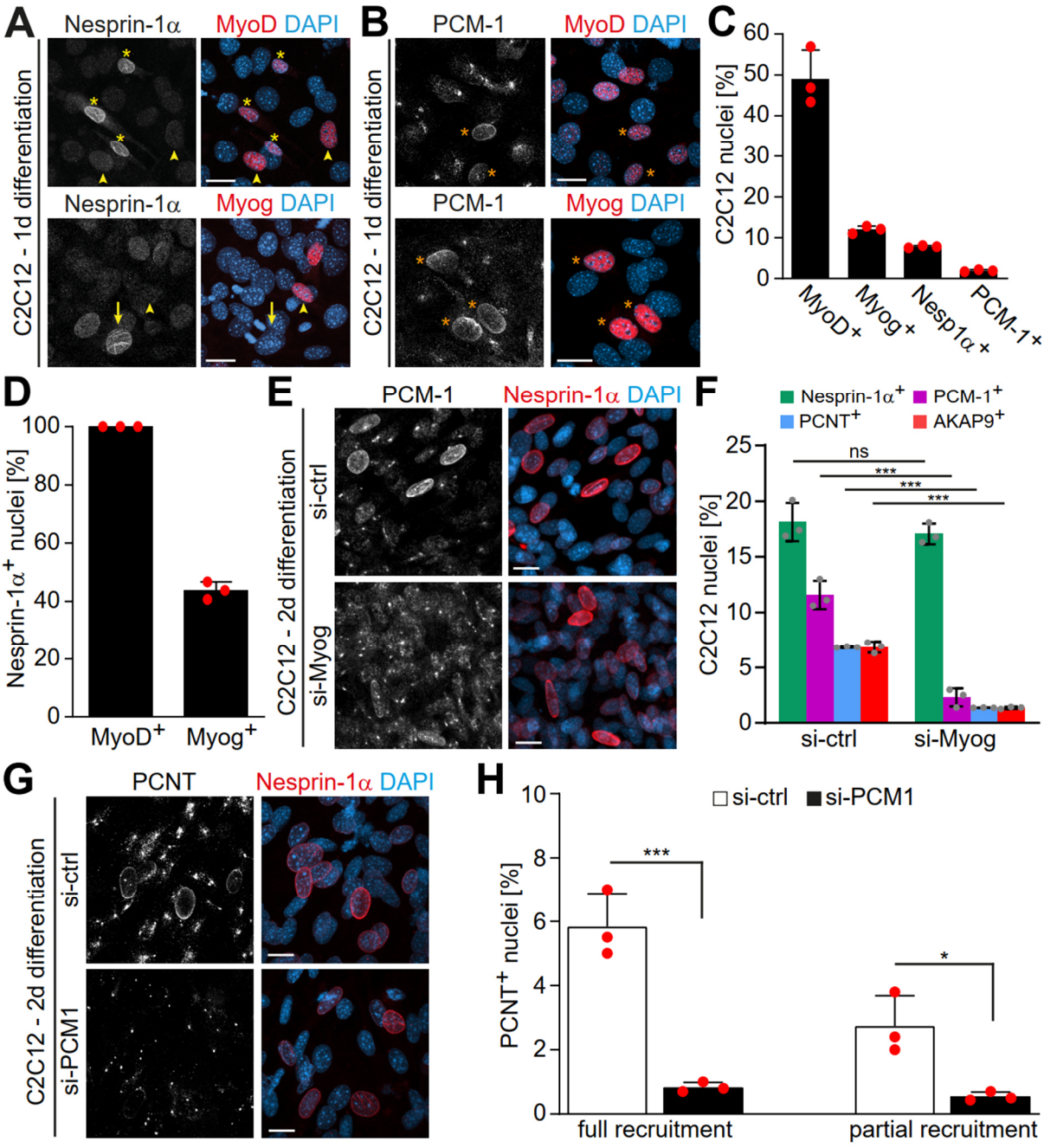

1233

1234

1235 **Figure 1. Myogenin is required for MTOC protein localization to the nuclear**
1236 **envelope.**
1237 **(A-B)** C2C12 cells were differentiated for one day and immunostained for the myogenic
1238 regulatory factors (MRFs) MyoD or myogenin (Myog) and nesprin-1α (A) or PCM-1 (B).
1239 Orange asterisks: MRF^+/$PCM\text{-}1^+$ nuclei; yellow asterisks: MRF^+/nesprin-$1\alpha^+$ nuclei;
1240 arrowheads: MRF^+/nesprin-$1\alpha^-$ nuclei; arrows: MRF^-/nesprin-$1\alpha^+$ nuclei. **(C)**
1241 Quantification of (A) and (B). **(D)** Quantification of MyoD and Myog in relation to
1242 nesprin-1α showing that not all nesprin-$1\alpha^+$ nuclei are myogenin$^+$. **(E-F)** C2C12
1243 myoblasts were transfected with negative control (si-ctrl) or myogenin siRNA (si-Myog)
1244 and differentiated for two days. Immunostaining (E) and subsequent quantification (F)
1245 shows that myogenin depletion affects nuclear envelope localization of PCM-1, PCNT,
1246 and AKAP9 but not of nesprin-1α. 95% CI of differences si-Myog vs. si-ctrl = -3.11% to
1247 0.98% (nesprin-$1\alpha^+$), -11.31% to -7.22% ($PCM\text{-}1^+$), -7.53% to 3.43% ($PCNT^+$), -7.52%
1248 to -3.42% ($AKAP9^+$). **(G-H)** C2C12 myoblasts were transfected with si-ctrl or PCM-1
1249 siRNA (si-PCM1) and differentiated for two days. PCNT was detected by
1250 immunostaining (G) and subsequent quantification (H) showed that PCM-1 depletion
1251 reduces $PCNT^+$ nuclei. 95% CI of differences si-PCM1 vs. si-ctrl = -6.6% to -3.4%
1252 (full), -3.78% to -0.59% (partial). Scale bars (A, B, E, G): 20 µm. Data (C, D, F, H) are
1253 represented as individual biological replicates (n = 3), together with mean ± SD.
1254 ns: $p > 0.05$. *: $p < 0.05$ ***: $p < 0.001$.
1255

Becker R *et al.*, Figure 2

Myogenin expression is sufficient to induce NE-MTOC formation in non-muscle cells.

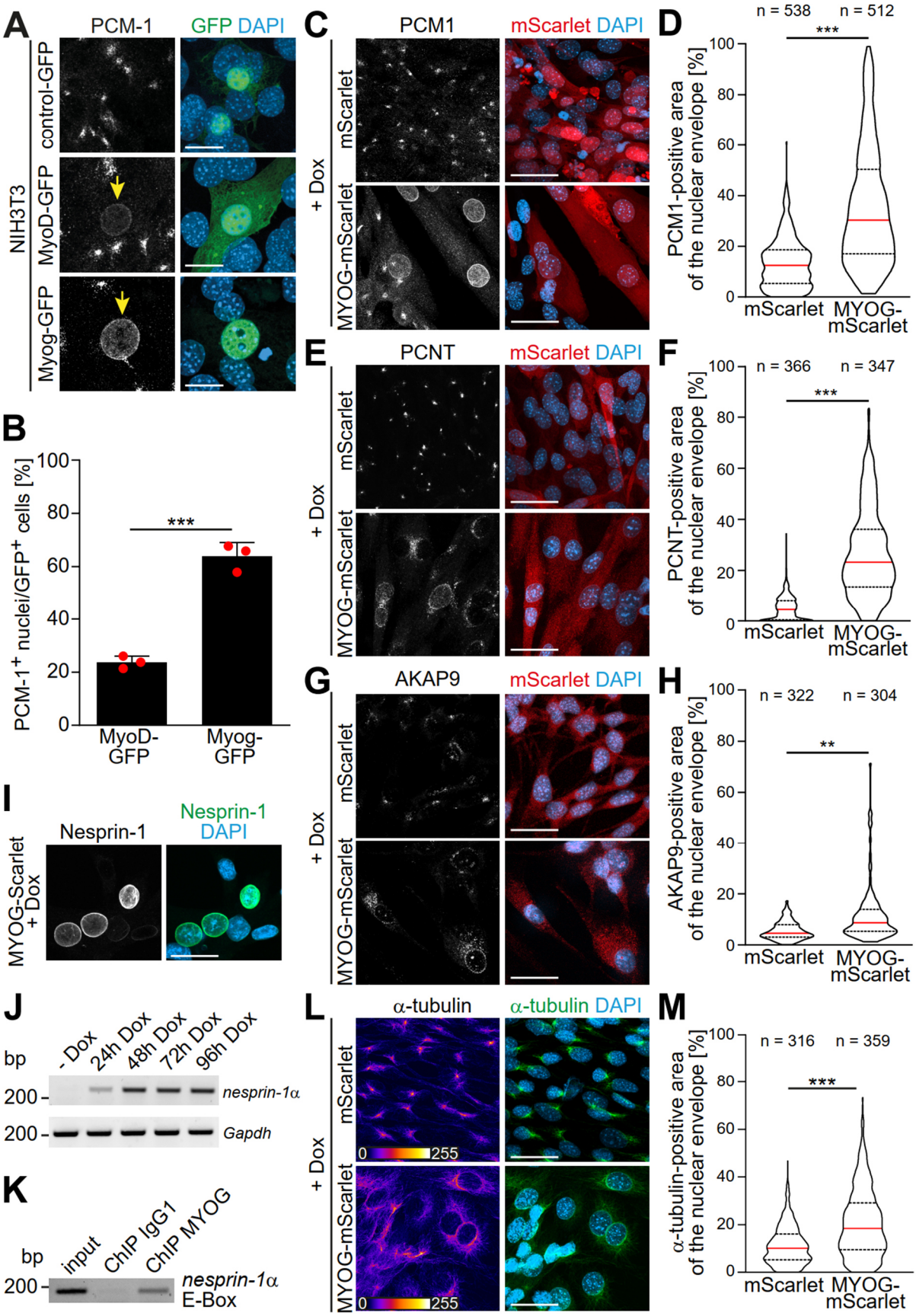

1256

1257 **Figure 2. Myogenin expression is sufficient to induce NE-MTOC formation in**
1258 **non-muscle cells.**
1259 **(A)** NIH3T3 fibroblasts were transfected with constructs encoding GFP, MyoD-GFP or
1260 myogenin-GFP (Myog-GFP). After three days, PCM-1 localization was assessed by
1261 immunostaining. Arrows indicate nuclei of transfected cells which have recruited
1262 PCM-1. Scale bars: 10 µm. **(B)** Quantification of (A) demonstrating that myogenin
1263 induces nuclear envelope localization of PCM-1 more efficiently than MyoD. Data are
1264 represented as individual biological replicates (n = 3), together with mean ± SD. ***: p
1265 < 0.001; 95% CI of difference Myog-GFP vs. MyoD-GFP = 30.99% to 49.22%. n = 3.
1266 **(C-H)** NIH3T3 Tet-ON mScarlet or MYOG-2A-mScarlet (MYOG-mScarlet) cells were
1267 treated with doxycycline (Dox) for three days. After immunostaining, nuclear envelope
1268 localization of PCM-1 (C-D), PCNT (E-F), and AKAP9 (G-H) was analyzed and
1269 quantified. Data are depicted as violin plots. Red line indicates the median, dotted lines
1270 indicate the 25% and 75% percentile. ***: p < 0.001. Scale bars: 20 µm **(I)**
1271 Immunostaining of MYOG-mScarlet cells treated with Dox for three days showing the
1272 presence of nesprin-1α^{+} nuclei. Scale bars: 20 µm **(J)** RT-PCR analysis of MYOG-
1273 mScarlet cells in the absence of Dox (-Dox) or treated with Dox for the indicated time
1274 points demonstrating that *nesprin-1α* is upregulated upon myogenin expression.
1275 *Gapdh* was used as equal input control. **(K)** ChIP-PCR analysis of Dox-treated MYOG-
1276 mScarlet cells using an anti-myogenin antibody or an IgG1 control showing that
1277 myogenin binds an E-box in the nesprin-1α promoter region. **(L-M)** Immunostaining of
1278 α-tubulin and subsequent quantification of nuclear envelope coverage after 30s of
1279 microtubule regrowth following cold-induced microtubule depolymerization in mScarlet
1280 or MYOG-mScarlet cells treated with Dox for three days. Data are depicted as violin
1281 plots. Red line indicates the median, dotted lines indicate the 25% and 75% percentile.
1282 ***: p < 0.001. Scale bars: 20 µm. N numbers indicate total number of analyzed nuclei
1283 pooled from three biological replicates.
1284

Becker R *et al.*, Figure 3

Myogenin expression attenuates the centrosomal MTOC.

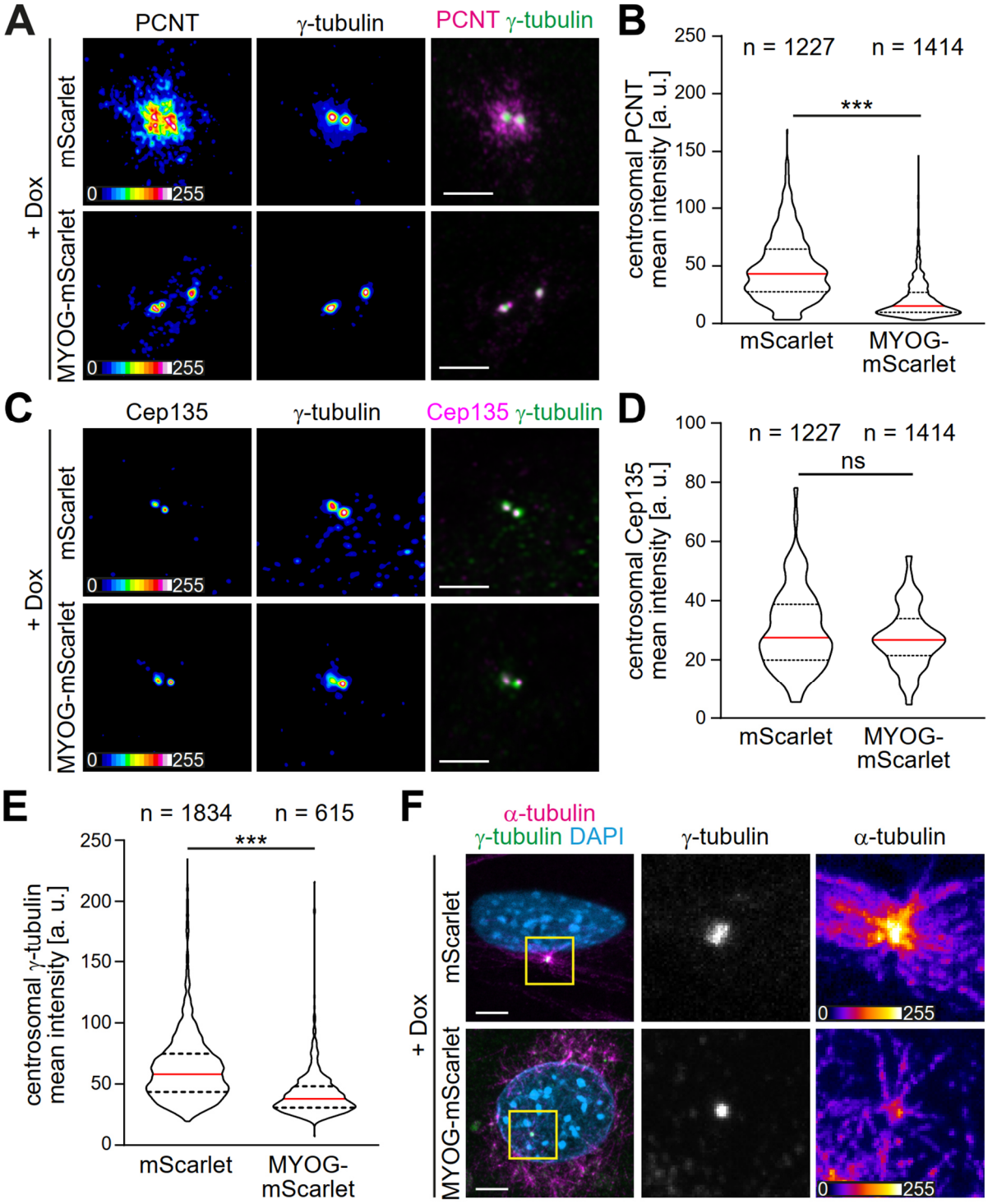

1285

1286

1287 **Figure 3. Myogenin expression attenuates the centrosomal MTOC.**
1288 **(A-E)** mScarlet or MYOG-mScarlet cells were stimulated with Dox for three days and
1289 PCNT (A), Cep135 (C), and γ-tubulin (A, C) were detected by immunostaining.
1290 Quantification shows that PCNT (B) and γ-tubulin (E) intensities at the centrosome are
1291 reduced upon myogenin induction while Cep135 intensity (D) is not significantly
1292 affected. Single channel images of Pcnt, γ-tubulin, and Cep135 are false-colored to
1293 visualize different intensities. Data are shown as violin plots. The red line indicates the
1294 median and dotted lines indicate the 25% and 75% percentile. ns: $p > 0.05$.
1295 ***: $p < 0.001$. Scale bars = 5 µm. N numbers indicate the total number of analyzed
1296 centrioles (γ-tubulin foci) pooled from four biological replicates. **(F)** Immunostaining of
1297 α-tubulin and γ-tubulin in Dox-stimulated mScarlet or MYOG-mScarlet cells after 30s
1298 of microtubule regrowth. Intensity-based color-coding of α-tubulin shows that
1299 microtubule growth from centrioles is reduced after myogenin induction. Scale bars:
1300 5 µm.
1301

Becker R *et al.*, Figure 4

The nesprin-1α interaction partner AKAP6 is a potential mediator of myogenin-induced NE-MTOC formation.

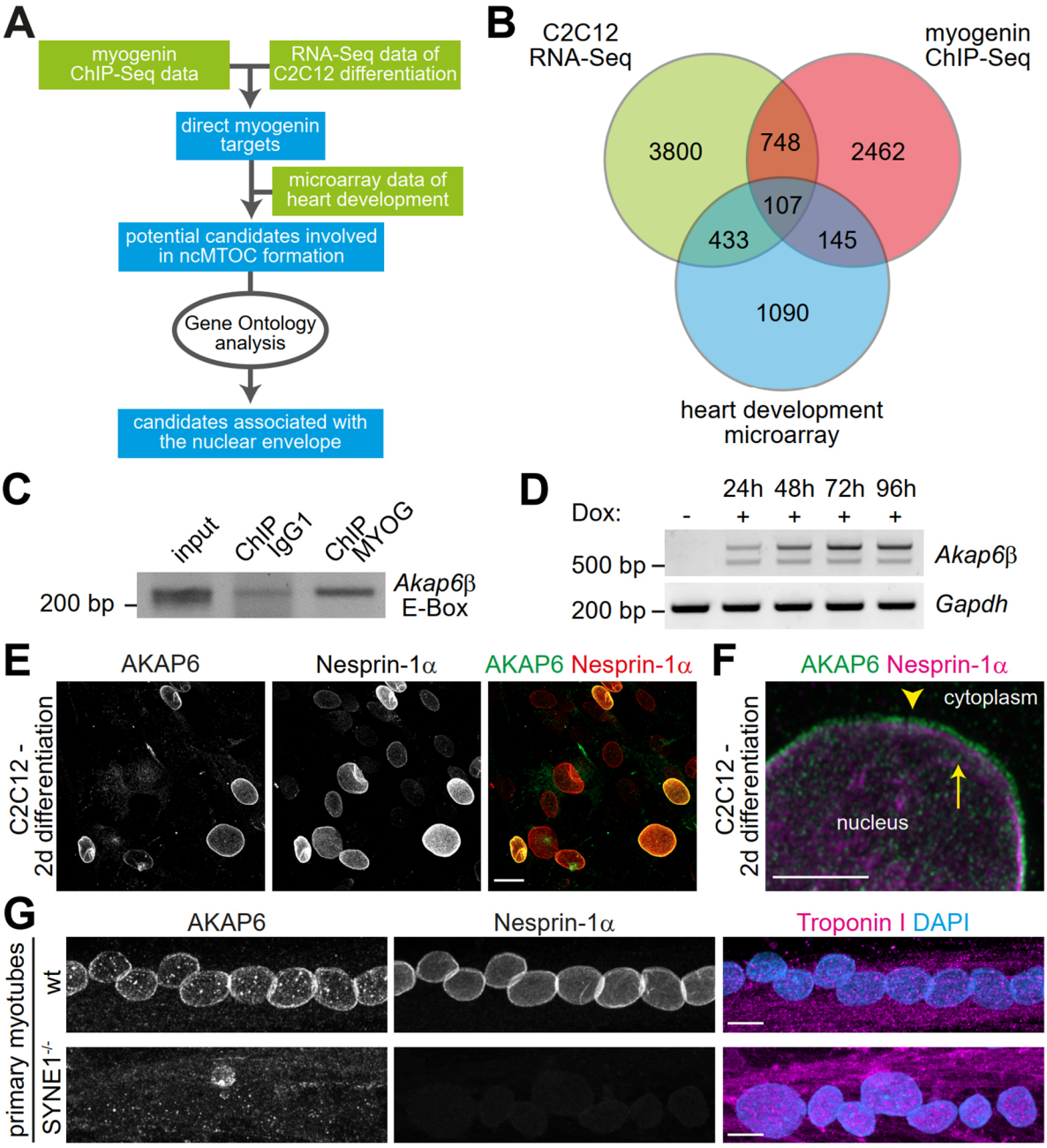

1304 **Figure 4. The nesprin-1α interaction partner AKAP6 is a potential mediator of**
1305 **myogenin-induced NE-MTOC formation.**
1306 **(A)** Scheme illustrating the bioinformatics workflow used to identify potential myogenin
1307 downstream candidates. **(B)** Venn diagram depicting the numbers of genes matching
1308 criteria for the individual data sets and for intersection of data sets. Criteria for
1309 Myogenin ChIP-Seq data (red): Genes where myogenin binding was detected at the
1310 promoter region; criteria for C2C12 RNA-Seq data (green) and for microarray data of
1311 rat heart development (blue): up-regulated genes. **(C)** ChIP-PCR analysis of Dox-
1312 treated MYOG-mScarlet cells using an anti-myogenin antibody or an IgG1 control
1313 showing that myogenin binds an E-box in the *Akap6*β-promoter region. **(D)** RT-PCR
1314 analysis of MYOG-mScarlet cells in the absence of Dox (-Dox) or treated with Dox for
1315 the indicated time points demonstrating that *Akap6β* is upregulated upon myogenin
1316 expression. The two bands for *Akap6β* derive from alternative splicing of the first exon
1317 of *Akap6β* which results in a ~200 bp insertion in the 5' untranslated region. *Gapdh*
1318 was used as equal input control. Please note that the same samples and *Gapdh* control
1319 were used as in Figure 2J. **(E)** C2C12 cells were differentiated for two days and
1320 immunostaining shows that all AKAP6^{+} nuclei are also nesprin-1α^{+}. Scale bar: 20 µm.
1321 **(F)** High resolution Airyscan image of (E). Arrowhead indicates AKAP6 localized at the
1322 cytoplasmic side of nesprin-1α signal. Arrow marks nesprin-1α that is localized at the
1323 nuclear side of AKAP6 signal. Scale bar: 0.5 µm. **(G)** Myoblasts from healthy donors
1324 (wt) and from patients carrying a mutation in the *SYNE1* gene (SYNE1$^{-/-}$) were
1325 differentiated for four days. Immunostaining analysis showed that loss of nesprin-1α is
1326 associated with loss of AKAP6 from the nuclear envelope in differentiated myotubes
1327 (troponin I). Scale bars: 10 µm.
1328

Becker R *et al.*, Figure 5

AKAP6 is required for the nuclear envelope localization of MTOC proteins.

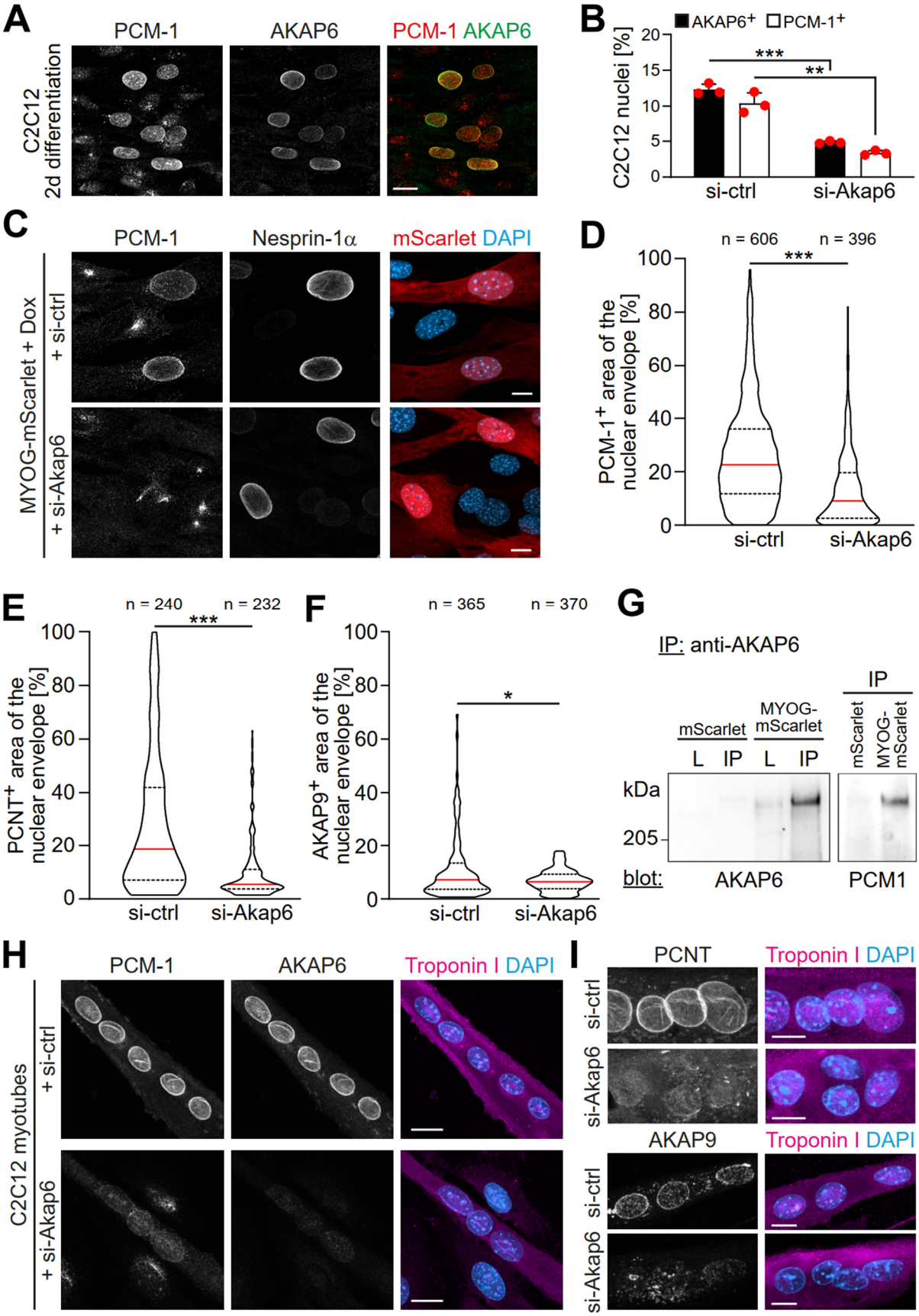

1329

1330 **Figure 5. AKAP6 is required for the nuclear envelope localization of MTOC**
1331 **proteins.**
1332 **(A)** C2C12 cells were differentiated for two days. Immunostaining shows that all
1333 PCM-1$^+$ nuclei are also AKAP6$^+$. **(B)** Quantification of AKAP6$^+$ and PCM-1$^+$ nuclei in
1334 C2C12 cells treated with negative control (si-ctrl) or Akap6 (si-Akap6) siRNA after two
1335 days of differentiation indicate that AKAP6 is required for nuclear envelope localization
1336 of PCM-1. Data are represented as individual biological replicates (n = 3), together with
1337 mean ± SD. 95% CI = 6.21% to 8.74%; 95% CI = 4.63% to 9.43%. **(C)** MYOG-mScarlet
1338 cells were treated with si-ctrl or si-Akap6 and subsequently treated with Dox for three
1339 days. Image analysis revealed that myogenin-induced localization of PCM-1 to the
1340 nuclear envelope is AKAP6-dependent. **(D)** Quantification of (C). **(E-F)** Quantification
1341 of PCNT (E) and AKAP9 (F) nuclear coverage in Dox-stimulated MYOG-mScarlet cells
1342 treated with si-ctrl or si-Akap6. **(G)** Co-Immunoprecipitation (IP) of PCM 1 from MYOG-
1343 mScarlet but not from mScarlet lysate (L) using an anti-AKAP6 antibody. **(H-I)** Enriched
1344 C2C12 myotubes (troponin I) were transfected with negative control (si-ctrl) or Akap6
1345 (siAkap6) siRNA and immunostaining demonstrates that AKAP6 is required for
1346 maintaining nuclear envelope localization of PCM-1 (H) as well as PCNT and AKAP9
1347 (I). Scale bars (A, H): 20 µm, (C, I): 10 µm. Data (D, E, F) are shown as violin plots.
1348 The red line indicates the median and dotted lines indicate the 25% and 75%
1349 percentile. N numbers indicate the total number of analyzed nuclei pooled from three
1350 biological replicates. *: $p < 0.05$. **: $p < 0.01$. ***: $p < 0.001$.
1351

Becker R *et al.*, Figure 6

AKAP6 is required for correct nuclear positioning in myotubes.

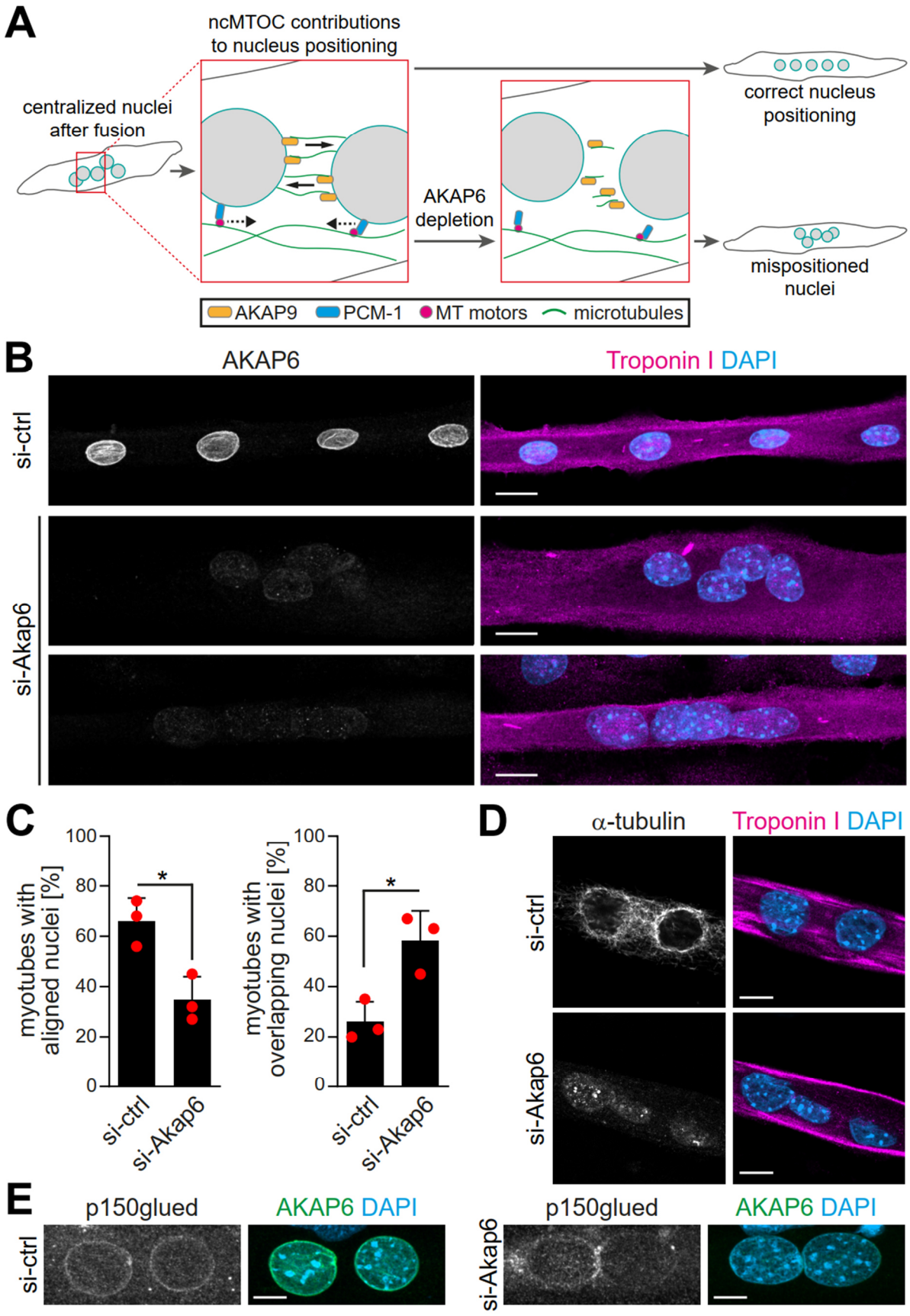

1352

1353 **Figure 6. AKAP6 is required for correct nuclear positioning in myotubes.**
1354 **(A)** Scheme illustrating the role of the NE-MTOC in myonuclear positioning and the
1355 potential impact of AKAP6 depletion. **(B)** Enriched C2C12 myotubes (troponin I) were
1356 transfected with negative control (si-ctrl) or Akap6 (si-Akap6) siRNA. The upper
1357 si-Akap6 panel shows a representative image of a myotube with misaligned nuclei, the
1358 lower si-Akap6 panel shows nuclei overlapping inside a myotube. **(C)** Quantification of
1359 (B). Data are represented as individual biological replicates (n = 3), together with mean
1360 ± SD. *: $p < 0.05$, 95% CI of difference si-Akap6 vs. si-ctrl = 10.42% to 52.25% (left
1361 graph); 95% CI = 9.65% to 55.02% (right graph). **(D)** Enriched C2C12 myotubes
1362 (troponin I) were transfected with si-ctrl or si-Akap6 and subsequently subjected to a
1363 nocodazole-based microtubule (α-tubulin) regrowth assay. Image analysis showed
1364 that AKAP6 depletion abrogated microtubule nucleation at the nuclear envelope. **(E)**
1365 Enriched C2C12 myotubes (troponin I) transfected with si-ctrl or si-Akap6 were
1366 immunostained for the dynein regulator p150glued. Image analysis showed that
1367 AKAP6 depletion reduces p150glued signal at the nuclear envelope. Scale bars (B):
1368 20 µm. (D): 10 µm. (E): 5 µm.
1369

Becker R *et al.*, Figure 7

Myogenin preferentially induces MTOC-associated isoforms of Syne1 and Akap6.

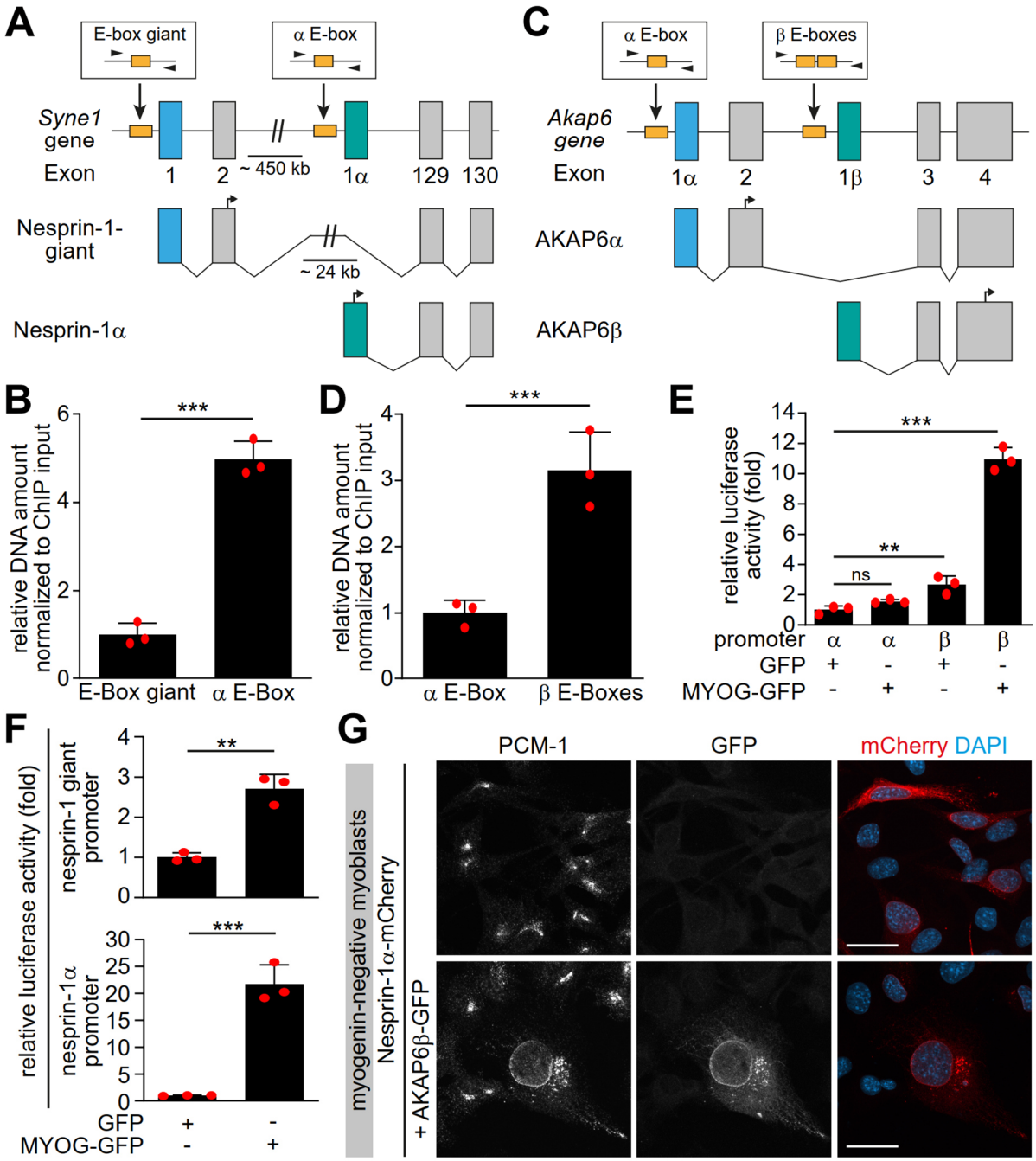

1370

1371

1372 **Figure 7. Myogenin preferentially induces MTOC-associated isoforms of *Syne1***
1373 **and *Akap6.***
1374 **(A, C)** Schematic representation of the murine *Syne1* (A) and *Akap6* (C) gene and
1375 derived transcripts. Exons are indicated by grey rectangles and the first exon of each
1376 transcript is marked by color. E-boxes (myogenin consensus sites) inside putative
1377 promoters are indicated as yellow boxes and small black arrows mark the primers used
1378 for qPCR. **(B, D)** Myogenin ChIP from Dox-stimulated MYOG-mScarlet cells followed
1379 by qPCR for the indicated E-boxes shows that myogenin preferentially binds the
1380 promoter regions upstream of *nesprin-1α* and *Akap6β* transcripts. **(E-F)** Luciferase
1381 assay testing the activity of the indicated *Akap6* (E) or *Syne1* (F) promoters in the
1382 presence of GFP or myogenin-GFP (MYOG-GFP). **(G)** Overexpression of nesprin-1α-
1383 mCherry alone or together with AKAP6β-GFP in undifferentiated (myogenin-negative)
1384 C2C12 myoblasts. Co-expression of nesprin-1α and AKAP6β is sufficient for nuclear
1385 envelope recruitment of endogenous PCM-1. Scale bars: 20 μm. Data (B, D, E, F) are
1386 represented as individual biological replicates (n = 3), together with mean ± SD. ns:
1387 $p > 0.05$. **: $p < 0.01$. ***: $p < 0.001$.
1388

Becker R *et al.*, Figure 8

Schematic overview of the role of myogenin and AKAP6 in NE-MTOC formation.

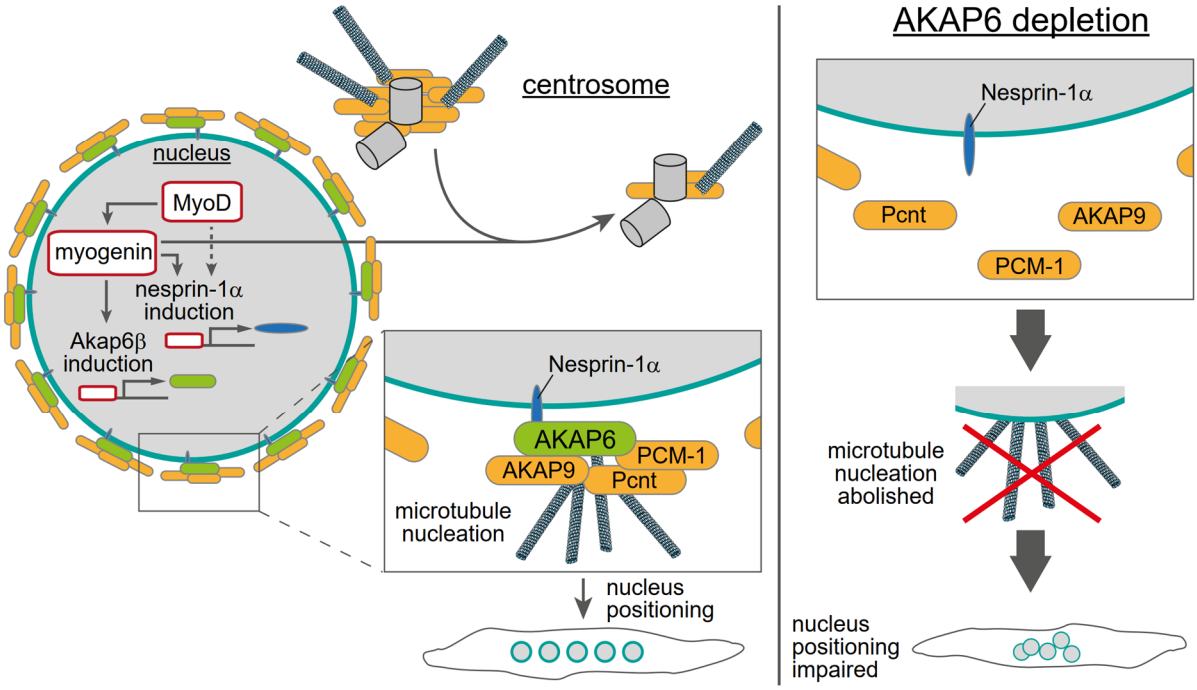

Figure 8. Schematic overview of the role of myogenin and AKAP6 in NE-MTOC formation.

Myogenin induces expression of AKAP6β which connects MTOC proteins like PCNT, AKAP9, and PCM-1 to the nuclear membrane protein nesprin-1α, whose expression can be induced by myogenin as well as MyoD. Depletion, overexpression, and co-immunoprecipitation experiments suggest that AKAP6β acts as an adapter between MTOC proteins and nesprin-1α. Yet, other proteins might be involved and the here presented protein complex at the nuclear envelope is hypothetical. At the same time, myogenin is sufficient to attenuate centrosomal MTOC function. AKAP6-dependent anchoring of MTOC proteins as well as microtubule nucleation from the nuclear envelope are required for correct positioning of nuclei inside differentiating myotubes.

1402 **Supplemental Figures**

Becker R *et al.*, Figure 1 - figure supplement 1
Intermediate stages of MTOC protein localization to the nuclear envelope.

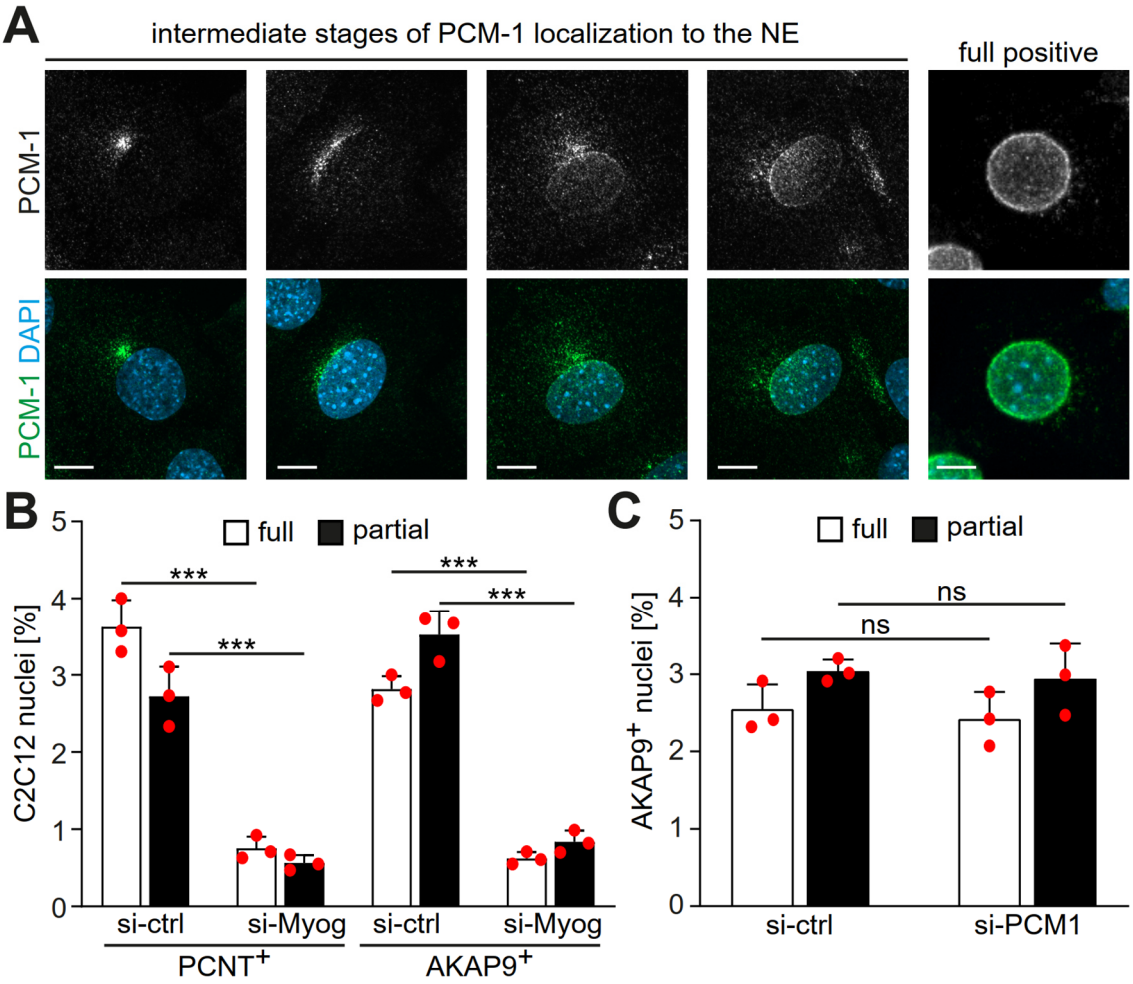

1403

1404 **Figure 1 – figure supplement 1. Intermediate stages of MTOC protein localization**
1405 **to the nuclear envelope.**

1406 **(A)** C2C12 cells were differentiated for 24h and PCM-1 was detected by
1407 immunostaining. Representative images of different intermediate stages of PCM-1
1408 recruitment are shown. Scale bar: 10 µm. **(B)** A more detailed quantification of PCNT$^+$
1409 and AKAP9$^+$ nuclei in differentiating C2C12 (treated as described in Figure 1F)
1410 showing that myogenin depletion affects also partial recruitment of PCNT and AKAP9.
1411 **(C)** C2C12 myoblasts were transfected with si-ctrl or PCM-1 siRNA (si-PCM1) and
1412 differentiated for two days. AKAP9 was detected by immunostaining and subsequent
1413 quantification showed that PCM-1 depletion does not affect AKAP9$^+$ nuclei. Data (B,
1414 C) are represented as individual biological replicates, together with mean ± SD. ns:
1415 $p > 0.05$. ***: $p < 0.001$. n = 3.

Becker R *et al.*, Figure 1 - figure supplement 2

PCM-1 exhibits a centrosomal localization pattern at nesprin 1+ nuclei in myogenin-depleted C2C12 cells.

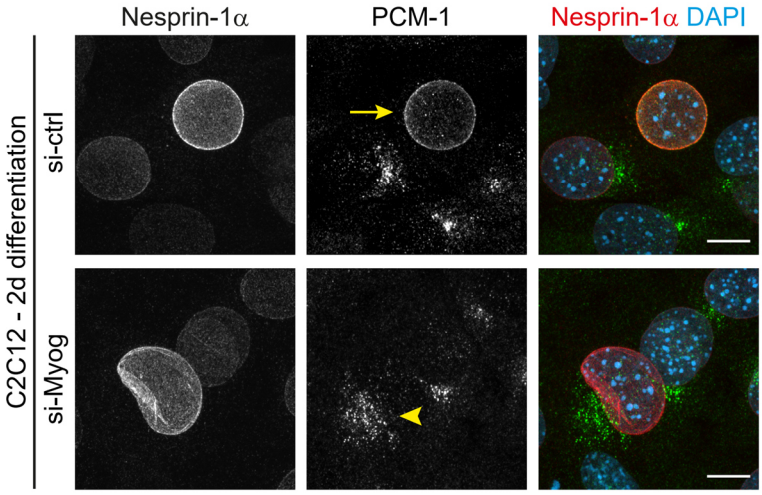

1416

1417 **Figure 1 – figure supplement 2. PCM-1 exhibits a centrosomal localization**
1418 **pattern at nesprin-1⁺ nuclei in myogenin-depleted C2C12 cells.**
1419 C2C12 myoblasts were transfected with negative control (si-ctrl) or myogenin siRNA
1420 (si-Myog) and differentiated for two days. In si-ctrl cultures, PCM-1 frequently localizes
1421 to the envelope of highly nesprin-1⁺ nuclei (yellow arrow). In si-Myog cultures, PCM-1
1422 can be found in a centrosomal pattern near nesprin-1⁺ nuclei (yellow arrowhead).
1423 Scale bar: 10 µm.

1424

Becker R *et al.*, Figure 2 - figure supplement 1

Myogenin is required for MyoD-induced nuclear envelope recruitment of PCM-1.

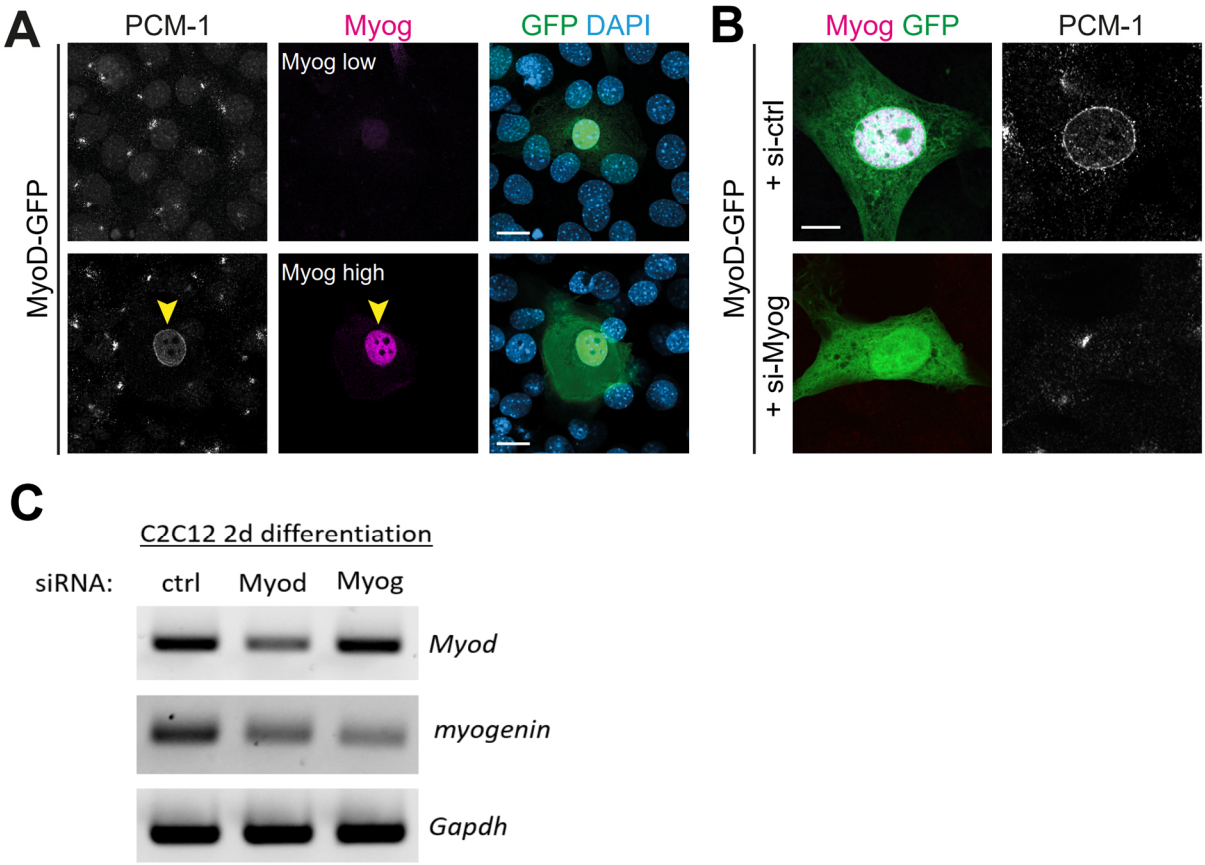

Figure 2 – figure supplement 1. Myogenin is required for MyoD-induced nuclear envelope recruitment of PCM-1.

(A) Three days after ectopic expression of MyoD-GFP in NIH3T3 fibroblasts, immunostaining revealed that nuclear PCM-1 localization is associated with high myogenin (Myog) expression (yellow arrowhead). **(B)** NIH3T3 cells were treated with negative control (si-ctrl) or myogenin (si-Myog) siRNA and 24 h later transfected with a construct encoding MyoD-GFP. Immunofluorescence staining indicates that myogenin is required for MyoD-induced PCM-1 nuclear recruitment. **(C)** C2C12 cells were transfected with the indicated siRNAs and differentiated for two days. RT-PCR analysis reveals that depletion of MyoD reduces myogenin levels in differentiating myoblasts but not *vice versa*. Scale bars (A, B): 10 µm.

Becker R *et al.*, Figure 2 - figure supplement 2

Myogenin targets are specifically precipitated in induced MYOG-mScarlet cells.

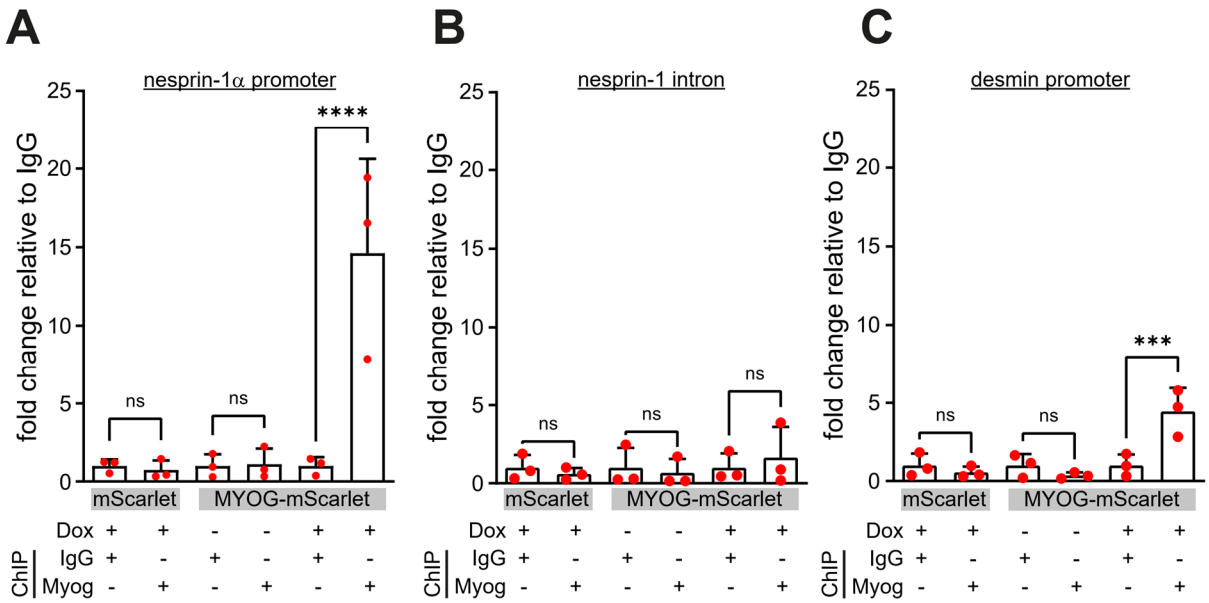

Figure 2 – figure supplement 2. Myogenin targets are specifically precipitated in induced MYOG-mScarlet cells.

ChIP was performed on the indicated lysates using the anti-myogenin antibody or an isotype control (IgG). The relative abundance of **(A)** the nesprin-1α promoter region, **(B)** an intronic region of nesprin-1 (negative control) or **(C)** the desmin promoter region (positive control) were determined by qPCR. Data are represented as individual biological replicates (n = 3), together with mean ± SD. ns: $p > 0.05$. ***: $p < 0.01$. ****: $p < 0.001$.

Becker R *et al.*, Figure 2 - figure supplement 3

Microtubule depolymerization in mScarlet and MYOG-mScarlet cells.

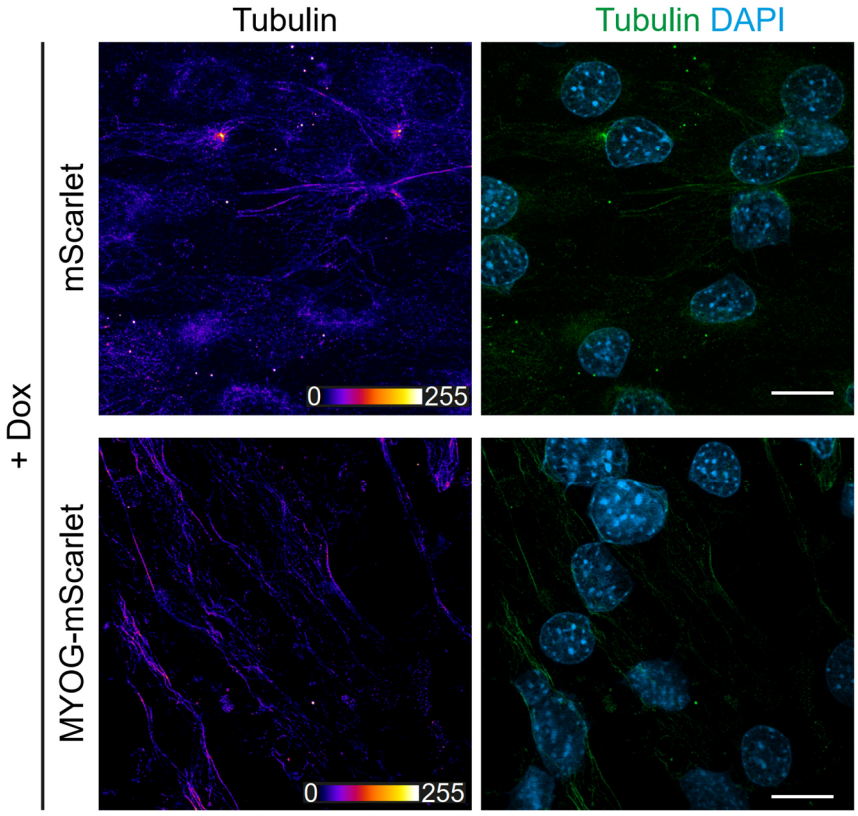

1448

1449 **Figure 2 – figure supplement 3. Microtubule depolymerization in mScarlet and**
1450 **MYOG-mScarlet cells.**

1451 Immunostaining of α-tubulin in mScarlet or MYOG-mScarlet cells treated with Dox for
1452 three days following cold-induced microtubule depolymerization without regrowth.
1453 Scale bar = 20 µm.

1454

Becker R *et al.*, Figure 4 - figure supplement 1

The myogenin antibody specifically precipitates the Akap6β promoter region in induced MYOG-mScarlet cells.

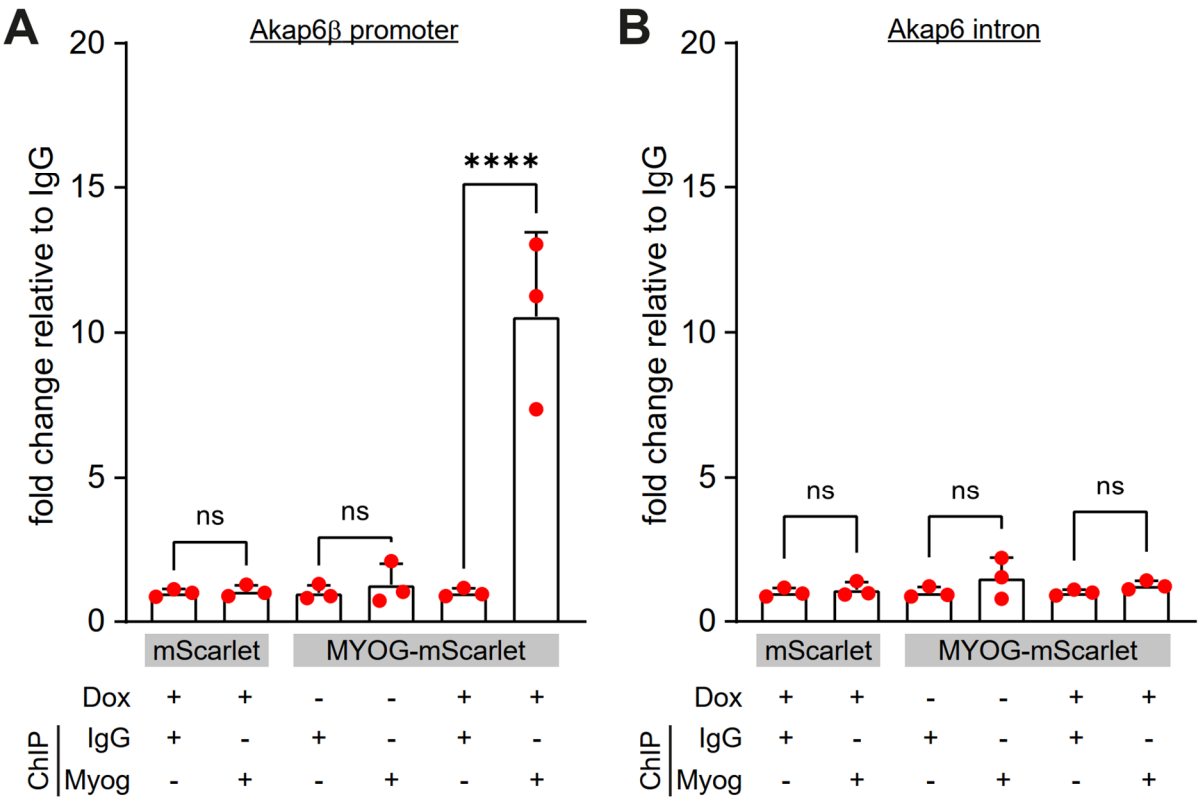

Figure 4 – figure supplement 1. The myogenin antibody specifically precipitates the Akap6β promoter region in induced MYOG-mScarlet cells.

Indicated lysates were probed using the anti-myogenin antibody or an isotype control (IgG). The relative abundance of **(A)** the Akap6β promoter region or **(B)** an intronic region of Akap6 was determined by qPCR. Data are represented as individual biological replicates (n = 3), together with mean ± SD. ns: $p > 0.05$. ****: $p < 0.001$.

Becker R *et al.*, Figure 4 - figure supplement 2

Quantification of nesprin-1α and AKAP6 signal at the nuclear envelope.

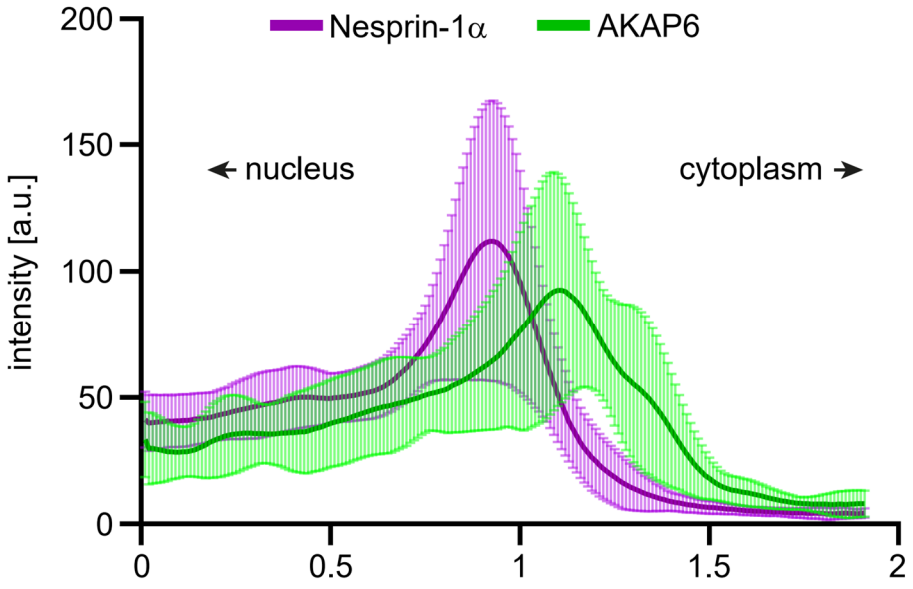

1463

1464 **Figure 4 – figure supplement 2. Quantification of nesprin-1α and AKAP6 signal**
1465 **at the nuclear envelope.**

1466 Differentiated C2C12 cells were immunostained for nesprin-1α and AKAP6. Signal
1467 intensity was quantified as line scan profiles across the nuclear envelope. Ten line
1468 scan profiles were obtained in regular intervals along the nuclear periphery and pooled
1469 from ten nuclei. Data are shown as mean ± SD.

1470

Becker R *et al.*, Figure 5 - figure supplement 1

AKAP6 depletion does not affect nesprin-1α.

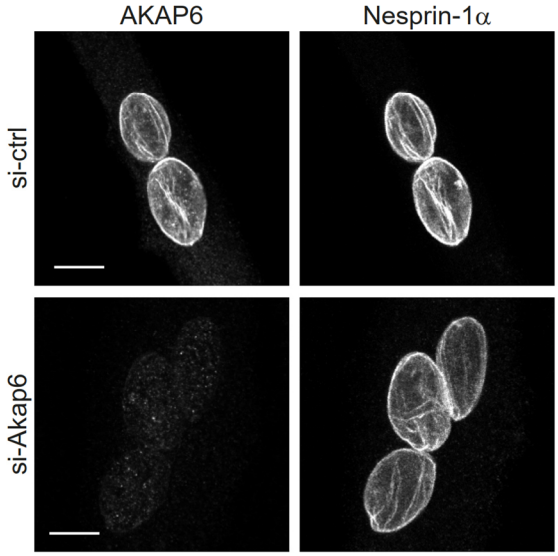

1471

1472 **Figure 5 – figure supplement 1. AKAP6 depletion does not affect nesprin-1α.**

1473 Enriched C2C12 myotubes were transfected with scrambled or Akap6-siRNA and

1474 immunostained for Akap6 and nesprin-1α. Scale bars: 10 µm.

1475

Becker R *et al.*, Figure 5 - figure supplement 2

AKAP6 or nesprin 1α depletion does not prevent centrosome attenuation in MYOG-expressing cells.

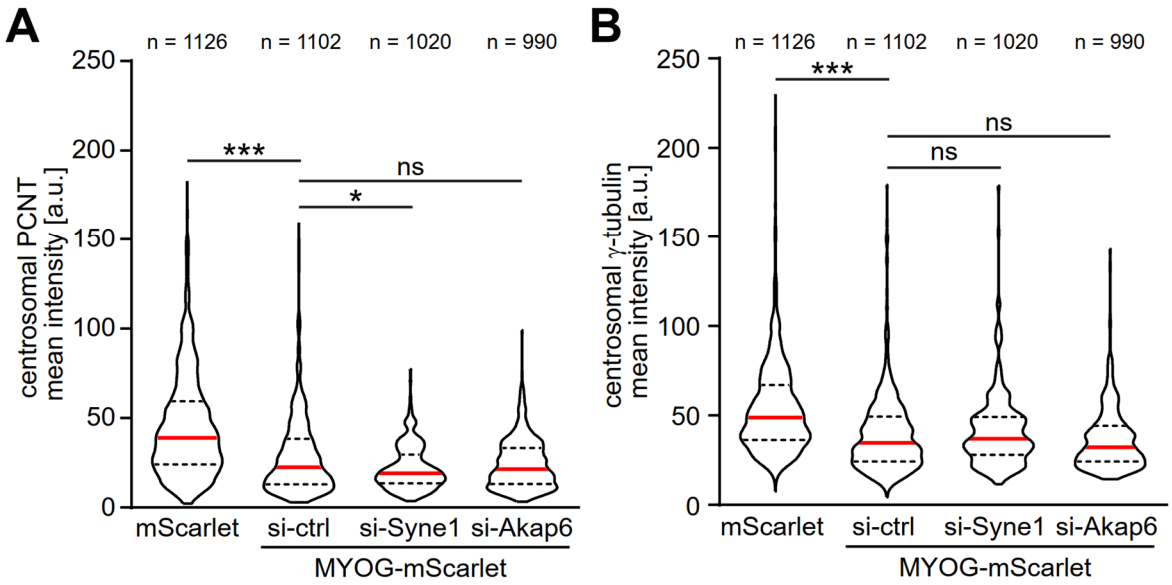

Figure 5 – figure supplement 2. AKAP6 or nesprin-1α depletion does not prevent centrosome attenuation in MYOG-expressing cells.

(A-B) mScarlet or MYOG-mScarlet transfected with the indicated siRNAs were stimulated with Dox for three days. PCNT (A) and γ-tubulin (B) immunostaining intensities were quantified. Data are shown as violin plots. The red line indicates the median and dotted lines indicate the 25% and 75% percentile. N numbers are the total number of analyzed centrioles pooled from three biological replicates. Note that here PCNT and γ-tubulin intensities were measured simultaneously.

Becker R *et al.*, Figure 5 - figure supplement 3

MyoD induces nesprin 1α and AKAP6.

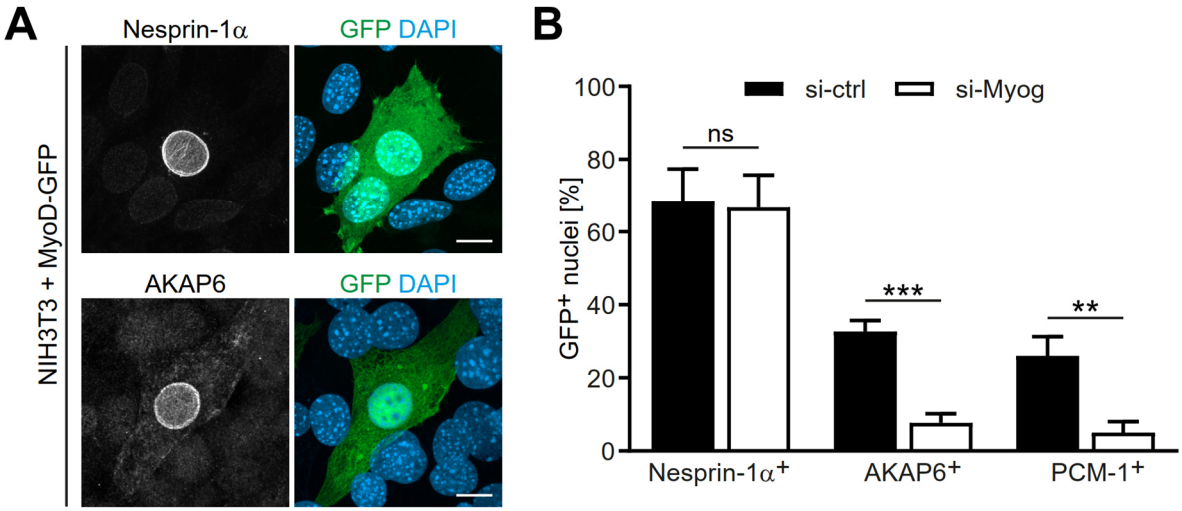

Figure 5 – figure supplement 3. MyoD induces nesprin-1α and AKAP6. **(A)** NIH3T3 cells were transfected with MyoD-GFP. Two days after transfection, nesprin-1α and AKAP6 were detected via immunostaining. Scale bar: 10 µm. **(B)** NIH3T3 cells were transfected with non-targeting siRNA (si-ctrl) or myogenin siRNA (si-Myog) and one day later transfected with MyoD-GFP. Indicated MTOC components were detected using immunostaining and positive nuclei were quantified. Data are represented as mean ± SD. n = 3. ns: $p > 0.05$. **: $p < 0.01$. ***: $p < 0.001$.

Becker R *et al.*, Figure 6 - figure supplement 1

AKAP6 depletion does not affect steady state microtubule organization but reduces detyrosinated microtubules.

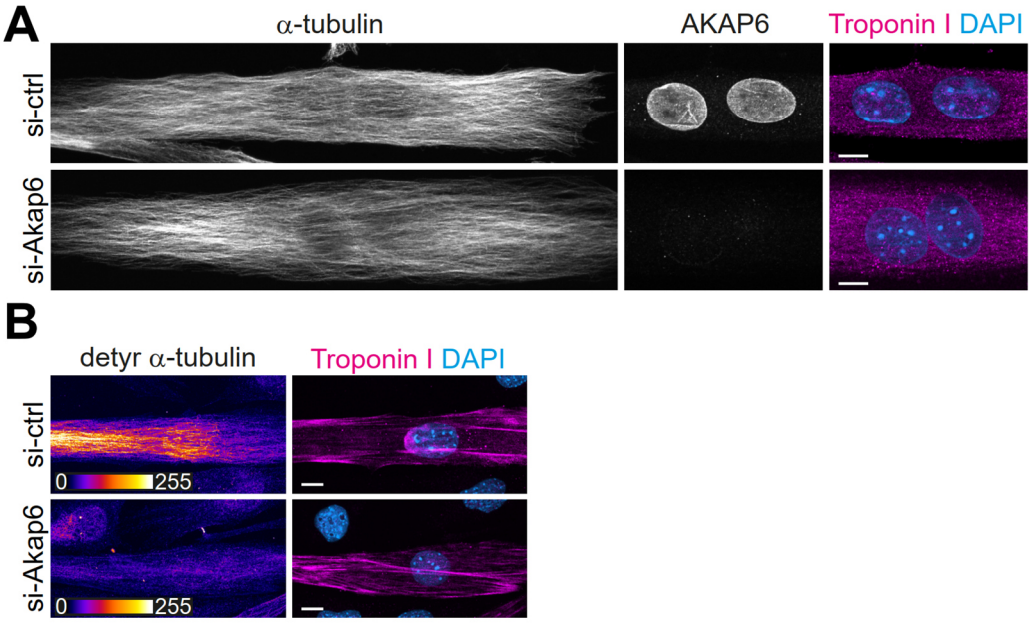

1495

1496 **Figure 6 – figure supplement 1. AKAP6 depletion does not affect steady state**
1497 **microtubule organization but reduces detyrosinated microtubules.**
1498 **(A-B)** Enriched C2C12 myotubes (troponin I) were transfected with negative control
1499 (si-ctrl) or Akap6 (si-Akap6) siRNA and subsequently analyzed for overall microtubule
1500 (α-tubulin) structure (A) or detyrosinated microtubules (detyr α-tubulin). Scale bars:
1501 10 µm.
1502

Becker R *et al.*, Figure 7 - Supplemental figure 1

Ectopic co-expression of nesprin-1α and AKAP6β is not sufficient for MTOC function at the nuclear envelope.

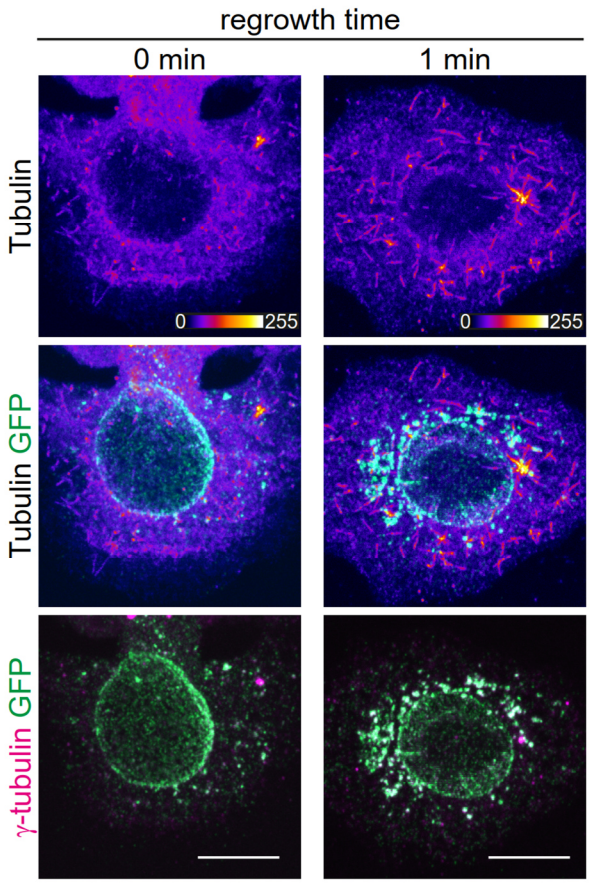

1503

1504 **Figure 7 – figure supplement 1. Ectopic co-expression of nesprin-1α and**
1505 **AKAP6β is not sufficient for MTOC function at the nuclear envelope.**
1506 Proliferating (myogenin-negative) C2C12 myoblasts were transfected with nesprin-1α-
1507 mCherry and AKAP6β-GFP. Two days after transfection, microtubule regrowth assays
1508 were performed. Scale bar: 10 µm.